

# Application of nanotechnologies for quantification measurement of nanoparticles from human cerebrospinal fluid: comparison of atomic force microscopy and tunable resistive pulse sensing

---

Vidović, Ivona

Master's thesis / Diplomski rad

2021

Degree Grantor / Ustanova koja je dodijelila akademski / stručni stupanj: **University of Rijeka / Sveučilište u Rijeci**

Permanent link / Trajna poveznica: <https://urn.nsk.hr/urn:nbn:hr:193:956840>

Rights / Prava: [In copyright](#) / [Zaštićeno autorskim pravom.](#)

Download date / Datum preuzimanja: **2024-04-23**



image not found or type unknown

Repository / Repozitorij:

[Repository of the University of Rijeka, Faculty of Biotechnology and Drug Development - BIOTECHRI Repository](#)



zir.nsk.hr



image not found or type unknown

UNIVERSITY OF RIJEKA  
DEPARTMENT OF BIOTECHNOLOGY  
University Graduate Programme  
*Medicinal chemistry*

Ivona Vidović

Application of nanotechnologies for quantification measurement of  
nanoparticles from human cerebrospinal fluid: comparison of atomic force  
microscopy and tunable resistive pulse sensing

Master's thesis

Rijeka, 2021

UNIVERSITY OF RIJEKA  
DEPARTMENT OF BIOTECHNOLOGY  
University Graduate Programme  
*Medicinal chemistry*

Ivona Vidović

Application of nanotechnologies for quantification measurement of  
nanoparticles from human cerebrospinal fluid: comparison of atomic force  
microscopy and tunable resistive pulse sensing

Master's thesis

Rijeka, 2021

Mentor: Assoc. Prof. MLadenka Malenica

Co-Mentor: Dr. sc. Marko Perčić

SVEUČILIŠTE U RIJECI  
ODJEL ZA BIOTEHNOLOGIJU  
Diplomski sveučilišni studij  
Medicinska kemija

Ivona Vidović

Primjena nanotehnologija za mjerenje koncentracije i promjera  
izvanstaničnih vezikula iz likvora čovjeka: usporedba mikroskopije  
atomske sile i opažanja pomoću podesivog otpornog pulsa

Diplomski rad

Rijeka, 2021.

Mentor: izv. prof. dr. sc. MLadenka Malenica

Komentor: dr. sc. Marko Perčić

## **Acknowledgements**

*I wish to express my utmost gratitude to mentor, Assoc. Prof. MLadenka Malenica, and co-mentor Dr. sc. Marko Perčić for their guidance and support. They provided constructive comments, warm encouragement and expert advice whenever were needed. I am sincerely grateful for your effort, patience, and knowledge you passed on to me.*

*I am grateful to my partner, friends and family. Thank you for your unconditional love, understanding and inexhaustible support you have given me throughout my schooling.*

Mentor: Assoc. Prof. MLadenka Malenica

Co-mentor: Dr. sc. Marko Perčić

The thesis was defended on the 1<sup>st</sup> of September, 2021, in front of a committee:

1. Assoc. Prof. Mirela Sedić, PhD
2. Assoc. Prof. Kristina Grabušić, PhD
3. Dr. sc. Marko Perčić
4. Assoc. Prof. MLadenka Malenica, PhD

The thesis has 51 pages, 5 figures, 1 table and 50 citations.

## Razvoj istraživačke infrastrukture na Kampusu Sveučilišta u Rijeci OBRAZAC ZA IZVJEŠĆIVANJE O KORIŠTENJU ZNANSTVENE OPREME

Projekt Sveučilišta u Rijeci „Razvoj istraživačke infrastrukture na Kampusu Sveučilišta u Rijeci“ financiran je iz Europskog fonda za regionalni razvoj (EFRR) u iznosu od 180.182.048,91 kn.

<b>Vrsta rada:</b>	Diplomski rad
<b>Datum:</b>	
<b>Institucija/e:</b>	Medicinski fakultet Sveučilišta u Rijeci Centar za mikro- i nanoznanosti i tehnologije (NANORI) – Sveučilište u Rijeci
<b>Naziv rada (HRV):</b>	Primjena nanotehnologija za mjerenje koncentracije i promjera izvanstaničnih vezikula iz likvora čovjeka: usporedba mikroskopije atomskih sila i opažanja pomoću podesivog otpornog pulsa
<b>Naziv rada (ENG):</b>	Application of nanotechnologies for quantification measurement of nanoparticles from human cerebrospinal fluid: comparison of atomic force microscopy and tunable resistive pulse sensing
<b>Sažetak:</b>	<p>Izvanstanične vezikule (IV) su membranske nanočestice koje se trenutno intenzivno proučavaju zbog njihove kvalitativne i kvantitativne promjene u patofiziološkim stanjima. Naime, IV-e izlučuju praktički sve stanice, a njihov molekularni sastav odražava vrstu i stanje stanica iz kojih potječu. Međutim, istraživanje IV-a je otežano zbog nedostatka metoda za preciznu i pouzdanu kvantifikaciju.</p> <p>Cilj istraživanja bio je poboljšati mjerenje veličine i koncentracije IV-a u njihovom prirodnom okruženju primjenom novih tehnologija koje mogu izravno mjeriti pojedinačne nanočestice. Takva se kvantifikacija dobiva opažanjem pomoću podesivog otpornog pulsa (engl. Tunable Resistive Pulse Sensing, TRPS) i mikroskopijom atomske sile (engl. Atomic Force Microscopy, AFM). Utvrđena je veličina i koncentracija IV-a iz likvora pacijenata s teškom ozljedom mozga, stanju u kojem su IV-e već opisane kako mijenjaju svoja fizička svojstva.</p> <p>TRPS mjerenja uzorka likvora pokazala su srednji promjer IV-a od <math>64,3 \pm 30,7</math> nm i koncentraciju od <math>1,3 \times 10^9</math> čestica/mL. Isti uzorak likvora korišten je za mjerenje AFM-om za koje je uveden novi protokol u načinu tapkanja kako bi se dobile slike IV-a u tekućem okruženju. Raspodjela promjera čestica izračunata je iz 10 slika veličine <math>1 \times 1 \mu\text{m}</math> s ukupno 170 nanočestica, što je rezultiralo srednjim promjerom od <math>59,2 \pm 22,1</math> nm i približnom koncentracijom od <math>1,7 \times 10^{10}</math> čestica/mL.</p> <p>Sveukupno, obje nanotehnologije rezultirale su sličnim vrijednostima promjera IV-a od oko 60 nm. Ipak, TRPS donosi kvantitativnu prednost u istodobnom mjerenju veličine i koncentracije IV-a. Ovo će istraživanje dodatno doprinijeti karakterizaciji kvantitativnih promjena nanočestica u biotekućinama.</p>
<b>Ključne riječi (HRV):</b>	izvanstanične vezikule, traumatska ozljeda mozga, likvor, mikroskopija atomskih sila, opažanje pomoću podesivog otpornog pulsa
<b>Ključne riječi (ENG):</b>	extracellular vesicles, traumatic brain injury, cerebrospinal fluid, atomic force microscopy, tunable resistive pulse sensing
<b>Autor rada:</b>	Ivona Vidović
<b>Mentor/i:</b>	izv. prof. dr. sc. MLadenka Malenica
<b>Komentor:</b>	dr. sc. Marko Perčić

## *Abstract*

Extracellular vesicles (EVs) are membranous nanoparticles that are currently intensively studied for their qualitative and quantitative changes in pathophysiological conditions. Namely, EVs are secreted by practically all cells and their molecular composition reflects the type and state of originating cells. However, research of EVs is hampered due to lacking methods for precise and reliable quantification.

The goal of this study was to improve EV size and concentration measurement in their natural environment by applying novel technologies able to directly measure individual nanoparticles. Such quantification is obtained by Tunable Resistive Pulse Sensing (TRPS) and Atomic Force Microscopy (AFM). The size and concentration of EVs were determined in cerebrospinal fluid (CSF) from patients with severe traumatic brain injury, a condition in which EVs have been previously described to change their physical properties.

TRPS measurements of the CSF sample showed a mean EV diameter of  $64.3 \pm 30.7$  nm and a concentration of  $1.3 \times 10^9$  particles/mL. The same CSF sample was used for the AFM measurement for which a novel protocol was introduced in tapping mode to obtain images in a liquid environment. Particle diameter distribution was calculated from 10  $1 \times 1 \mu\text{m}$  images containing 170 nanoparticles, resulting in a mean diameter of  $59.2 \pm 22.1$  nm, and a concentration approximation of  $1.7 \times 10^{10}$  particles/mL.

Taken together, both nanotechnologies resulted in similar EV diameter values of around 60 nm. Yet, TRPS brings a quantitative advantage in a simultaneous measurement of EV size and concentration. This research will further contribute to the characterisation of quantitative changes of nanoparticles in biofluids.

**Key words:** extracellular vesicles, traumatic brain injury, cerebrospinal fluid, atomic force microscopy, tunable resistive pulse sensing.



## Sažetak

Izvanstanične vezikule (IV) su membranske nanočestice koje se trenutno intenzivno proučavaju zbog njihove kvalitativne i kvantitativne promjene u patofiziološkim stanjima. Naime, IV-e izlučuju praktički sve stanice, a njihov molekularni sastav odražava vrstu i stanje stanica iz kojih potječu. Međutim, istraživanje IV-a je otežano zbog nedostatka metoda za preciznu i pouzdanu kvantifikaciju.

Cilj istraživanja bio je poboljšati mjerenje veličine i koncentracije IV-a u njihovom prirodnom okruženju primjenom novih tehnologija koje mogu izravno mjeriti pojedinačne nanočestice. Takva se kvantifikacija dobiva opažanjem pomoću podesivog otpornog pulsa (engl. *Tunable Resistive Pulse Sensing, TRPS*) i mikroskopijom atomske sile (engl. *Atomic Force Microscopy, AFM*). Utvrđena je veličina i koncentracija IV-a iz likvora pacijenata s teškom ozljedom mozga, stanju u kojem su IV-e već opisane kako mijenjaju svoja fizička svojstva.

TRPS mjerenja uzorka likvora pokazala su srednji promjer IV-a od  $64,3 \pm 30,7$  nm i koncentraciju od  $1,3 \times 10^9$  čestica/mL. Isti uzorak likvora korišten je za mjerenje AFM-om za koje je uveden novi protokol u načinu tapkanja kako bi se dobile slike IV-a u tekućem okruženju. Raspodjela promjera čestica izračunata je iz 10 slika veličine  $1 \times 1 \mu\text{m}$  s ukupno 170 nanočestica, što je rezultiralo srednjim promjerom od  $59,2 \pm 22,1$  nm i približnom koncentracijom od  $1,7 \times 10^{10}$  čestica/mL.

Sveukupno, obje nanotehnologije rezultirale su sličnim vrijednostima promjera IV-a od oko 60 nm. Ipak, TRPS donosi kvantitativnu prednost u istodobnom mjerenju veličine i koncentracije IV-a. Ovo će istraživanje dodatno doprinijeti karakterizaciji kvantitativnih promjena nanočestica u biotekućinama.

**Ključne riječi:** izvanstanične vezikule, traumatska ozljeda mozga, likvor, mikroskopija atomskih sila, opažanje pomoću podesivog otpornog pulsa.

# Contents

1. Introduction.....	11
1.1 Application of nanotechnologies in characterisation of EVs from human biofluids.....	11
1.2 Tunable Resistive Pulse Sensing .....	13
1.2.1 Principle and Izon's qNano configuration .....	14
1.2.2 Optimal condition settings .....	16
1.3 Atomic force microscopy .....	16
1.3.1 Principle and Bruker's SPM configuration .....	17
1.3.2 Operating modes.....	19
1.3.3 Probe selection for investigating biofluids in tapping mode .....	21
1.4 TRPS and AFM techniques in EV characterisation .....	22
2. The goal .....	25
3. Materials and methods .....	26
3.1 Sample collection .....	26
3.2 Tunable Resistive Pulse Sensing .....	26
3.2.1 Chemicals and reagents .....	26
3.2.2 Polystyrene standards .....	26
3.2.3 Solution and sample preparation.....	27
3.2.4 Instrument settings and analysis .....	27
3.3 Atomic Force Microscopy .....	28
3.3.1 NanoScope Analysis.....	29
3.3.2 Gwyddion.....	29
3.3.3 Concentration approximation.....	30
3.4 Statistical analysis .....	30
4. Results .....	31
4.1 Tunable resistive pulse sensing measurements with NP80 and NP100 nanopore of cerebrospinal fluid .....	31

4.2 Stability of tunable resistive pulse sensing measurements for cerebrospinal fluid .....	33
4.3 Image processing protocol with representative atomic force microscopy images of cerebrospinal fluid .....	35
4.4 Size distribution of nanoparticles in cerebrospinal fluid obtained after tunable resistive pulse sensing and atomic force microscopy measurements	37
5. Discussion.....	39
6. Conclusion .....	45
7. Bibliography .....	46
8. <i>Curriculum vitae</i> .....	49

## 1. Introduction

### **1.1 Application of nanotechnologies in characterisation of EVs from human biofluids**

Nanotechnological solutions are preparing to be implemented for future large-scale diagnostics, complex disease therapeutics and personalized medicine. The biological structure which has a potential to be the basis for revealing pathophysiological conditions in the future clinical approach are extracellular vesicles (EVs) [1]. Rapidly gaining momentum, these membraneous nanoparticles (NPs) range in size from 30 nm to 5  $\mu$ m [2]. EVs ensure intercellular communication by reflecting the state of the parental cell with their bioactive cargo. Theranostic<sup>1</sup> EV abilities have been investigated in biofluids like blood, urine, saliva, cerebrospinal and amniotic fluid among others [1]. Still, potential widespread applications in clinical settings are restricted by the Food and Drug Administration (FDA) and other regulatory agencies due to unstandardised methods of EV isolation and analysis [2]. The lack of uniformity in the field is own to several factors. Not only concentration, size and EV content vary among different biofluids, but also diseases, use of medications, age, gender, general lifestyle, dietary habits, sample handling and different nanotechnological techniques used influence the final EV content [3]. As an example, in a pathophysiology of traumatic brain injury (TBI), cells produced more EV volume than in a healthy state [4]. Yet, there are still contradictory evidence on their physical parameters that call on conducting further studies [4,5]. To investigate such differences, necessary is to look at nanotechnologies used in EV investigations from biofluids. Nanotechnologies can be roughly divided in microscopical and non-microscopical techniques. Microscopical most often provide single-cell characterisation with the morphological differences, and non-microscopical are usually high-throughput and can more easily provide quantitative information of a more diverse group of

---

<sup>1</sup> a combination of diagnostics and therapy

NPs, such as concentration and size distribution. Most common microscopical methods used in characterisation of EVs from biofluids are electron microscopy (EM) and atomic force microscopy (AFM). In the last decades, EM was considered a gold standard for EV visualisation [6]. EM uses electrons scattered or transmitted through the sample, using the electron property of having shorter than a photon wavelength, thus producing a picture of high-resolution. Most powerful EM can distinguish the EV presence in isolate, and identify protein aggregates up to 50 pm in subatomic resolution [7]. However, its operation in vacuum, inability to determine EV concentration, and multistep sample preparation that can cause structural modifications make EM less appealing as a technique of choice [3]. At the same time, the AFM also represents a well-established technique, with investigations of EVs gaining attention in the last decade. Whilst EM relies on the electron beam pathway, AFM senses sample's surface by measuring interaction forces between the probing tip and a sample. Similar in reaching a picometric resolution in its most advanced design, the main advantage of AFM over EM is enabling measurement of EVs in their native condition. Beside liquid, it provides measurement in different conditions, like vacuum and ambient air, with low force tapping modes principally aimed for soft biological samples. Sample preparation is minimised and can include tip functionalisation for further EV subgroup separation [8]. One of the biggest downsides of AFM is generating scanned images in the order of micrometers, in comparison with EM scanned images in the order of millimeters [9]. The latest developed AFMs have evolved to compensate for past shortcomings – automated not requiring as much of a expertise, being much faster in scanning, and reaching any point on 200 mm sample [10]. Still, resolution and image quality are dependent on tip sharpness and optimising of imaging parameters for individual samples. Looking at non-microscopical techniques for EV investigation, Vogel et al. (2021) recently compared six most commonly used methods for obtaining quantitative EV characteristics from biofluids [11]. Researchers compared light scattering techniques like nanoparticle tracking analysis (NTA) and

more recently developed techniques based on electrical impedance like tunable resistive pulse sensing (TRPS). NTA is the most common method used in describing NP size and concentration. NTA detects particles' Brownian motion by recording scattered light of the particles. NTA demonstrated more precise EV sizing than similar method, dynamic light scattering. However, in comparison with TRPS, it does not provide enough resolution to distinguish polydispersed EV classes. When particles of known sizes were compared in a trimodal mixture, TRPS fully resolved the proportion of 60 nm subpopulation while NTA severely underestimated it [11]. At the same time, TRPS is a technique that acquires information from ionic current blockades and controls its lowest detection range by the size-tunable nanopore. Beside being able to resolve populations in multimodal samples, TRPS uses much smaller sample volume (35  $\mu$ l versus a few hundreds  $\mu$ l in NTA). Unlike NTA, where the optical properties of NPs and dispersant are needed before analysis, TRPS requires minimal knowledge of NP properties before analysis. The downsides include unstable measurements that influence user experience, which may be overcome with the latest semi-automated product that does not rely on user inputs or instrument settings [12].

## **1.2 Tunable Resistive Pulse Sensing**

TRPS is a high-throughput nanoparticle characterisation technique that enables simultaneous size and concentration measurement. It measures particles from 30 nanometers to 20 micrometers in size, and  $10^5$  to  $10^{11}$  particles per milliliter in concentration [13]. The method is developed from the Coulter impedance principle. Influenced by the atomic bombs detonated over Hiroshima and Nagasaki in 1945., Wallace H. Coulter was motivated to improve and simplify his principle used for blood cell analysis. In case of nuclear war, it would provide rapid blood screening for large populations. The principle relies on particle-by-particle measurement of disturbances in the electric field while particles pass through a micro-channel.

Measurement requirements that Coulter identified were that particles should be suspended in a conducting liquid, the electrical field should be physically constricted so that the particle movement causes detectable current changes, and particles should be diluted enough to pass one at the time through the constriction, preventing artifacts [14].

### 1.2.1 Principle and Izon's qNano configuration

Tunable resistive pulse sensing is an adapted version of Coulter principle predominantly commercialized in the field of nanomedicine for EV, virus, DNA, protein complex, liposome, and drug delivery nanoparticle detection [15–17]. The main difference introduced in TRPS are elastomeric membranes with size adjustable ("tunable") micro-sized hole (Figure 1.D).

The principle relies on the Coulter approach for cell-sensing and single particle detection, with added value for the detection of a larger size range carried out by the size tuning mechanism. After nanopore is attached to the crucifix, electrolyte solution is added to either side of the pore. Both upper and lower fluid cell contain silver/silver chloride (Ag/AgCl) electrodes, below and above the membrane (Figure 1.A) [17]. By applying a voltage, electrodes excite electrolyte ions. By moving between the electrodes and through the nanopore, ions create baseline current flow. The sample is added to the upper chamber. Variable Pressure Module (VPM) is connected with the upper fluid cell via the transparent polymer tubing (Figure 1.B). A combination of voltage and pressure influences the speed of both charged and uncharged particles and drives them through the aperture. While passing through the pore, each particle causes an increase in electrical resistance, generating a transient decrease of the current, or a blockade signal [18]. These blocking events are detected by customized electronics in the base of the Izon qNano Gold instrument (Izon Science Ltd, Christchurch, New Zealand) [20]. Blockages are manifested as downward spikes in the current record (Figure 1.C). From the blockage events,

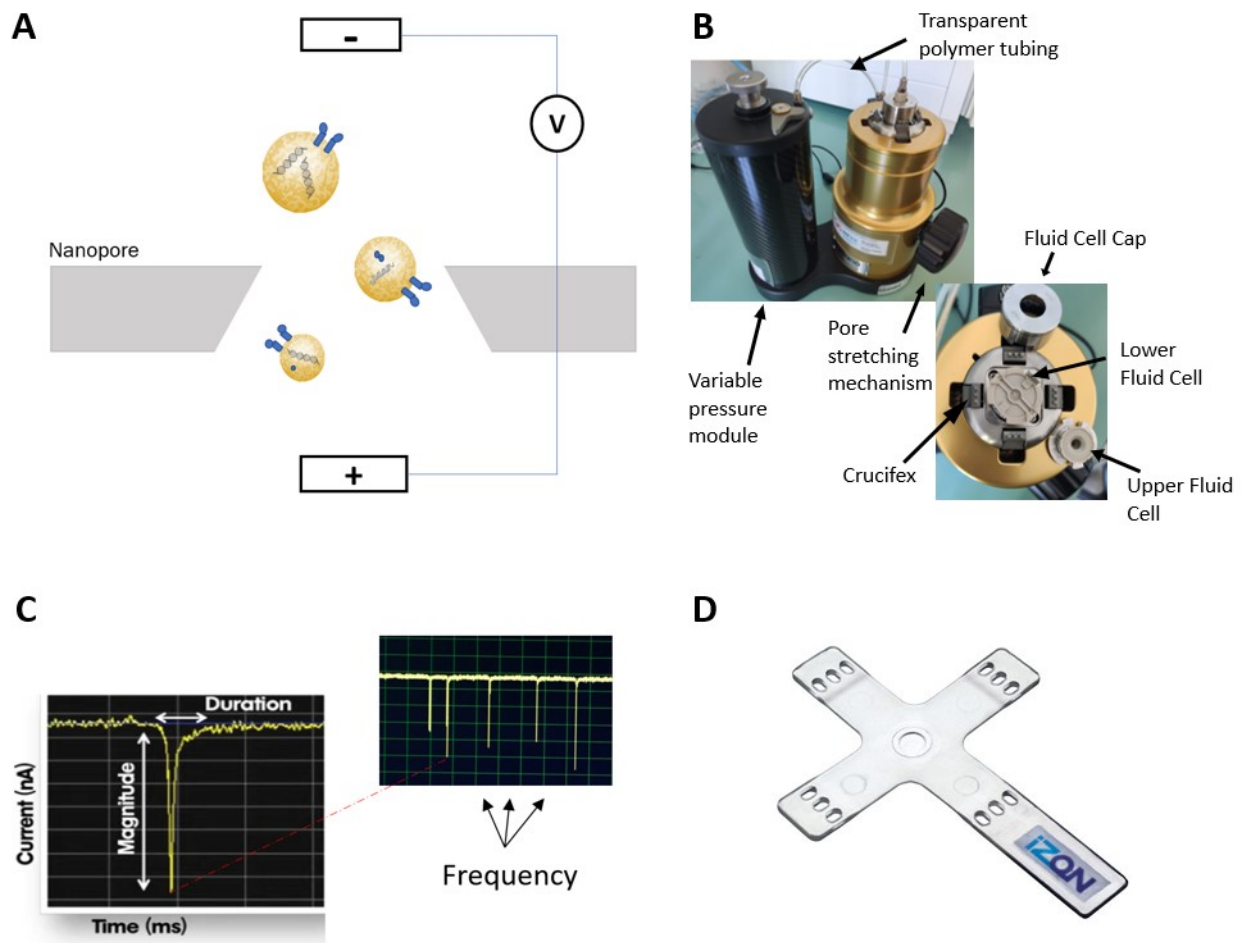


**Figure 1.** A. TRPS principle. The voltage applied across the nanopore filled with electrolyte establishes ionic current. EVs block the background current while passing through the pore, thus creating signal blockades. B. Izon's TRPS device configuration - qNano Gold. C. Obtained signals are translated into quantitative data - blockade height (magnitude) determines the particle size. Signal duration, the time taken for particle to pass the pore aperture, is converted into particle charge (zeta potential). The particle's concentration in the sample is determined by the signal's frequency. D. Izon's thermoplastic polyurethane nanopore. A. Modeled from Maas et al. [19], C. and D. retrieved and modified from [16].

particle size, charge and concentration can be calculated. Blockade height (magnitude) is directly proportional to the particle's volume, from blockade duration can be calculated the surface charge, and blockage frequency determines the sample's concentration (Figure 1.C). First, calibration particles of known size, concentration, and surface charge are measured. By comparison with the calibration particles, sample's parameters are



converted into respective particle properties and quantified by the application software.

### 1.2.2 Optimal condition settings

System stability issues are a major limitation of Coulter counter style devices. Instabilities occur when particles stick to nanopore surface, or when larger particles become stuck in the nanopore entirely blocking it. To lower the incidence of such issues, parameters like baseline current, pressure, root mean square (RMS) noise and rate plots can be monitored for instabilities [16]. A combination of pressure, voltage and optimised dilution should create baseline current of around 110 nA and RMS noise not higher than 15 pA. Otherwise, RMS higher than recommended, may cause smaller particles not to be detected, and hence, skew the results [16]. One of the biggest challenges during measurement can come from the aggregation of smaller NPs (<100 nm). One of the manufacturer's recommendations for smaller nanopores (NP80, NP100) is an application of a stronger electrolyte solution (2x phosphate buffer tablets, PBS) to improve the signal-to-noise ratio. Each particle has an ionic cloud that surrounds it. Using the higher ionic strength (buffer ions) can lower the particles' aggregation rate since there is a larger cushion of space between them [13]. Further, to reduce the occurrence of blockages and unwanted pore-modifications, Izon developed nanopore coating solution (Izon Science Ltd, Christchurch, New Zealand). Mostly used in biological samples, it is a protein-free PBS-based formation that minimizes unwanted binding, consequently increasing measurement stability [21].

## 1.3 Atomic force microscopy

Atomic force microscopy was invented in 1985., arising from a Nobel-prize winning scanning tunneling microscopy (STM) three years earlier by Binnig et al [22]. The STM was a breakthrough in studying surface with a spatial

resolution down to an atomic one. Measuring the tunneling<sup>2</sup> current between a metal needle and a conducting sample [23], STM provided a foundation for scanning probe microscopy (SPM) [24]. AFM was brought primarily by the need for imaging biological samples, that have poor electron conductivity [25]. The original AFM consisted of a diamond shard attached to a strip of gold foil, with diamond tip creating measurable interatomic van der Waals forces by the direct contact with the surface [22]. Nowadays, AFM provides new insights in physical, chemical, biological, and medical research. It evolved into a powerful technique capable of not only extracting information about 3D surface topography, but also surface properties such as stiffness, adhesion, conductivity and friction among others.

#### 1.3.1 Principle and Bruker's SPM configuration

The AFM uses a nanometer-sized tip attached to oscillant lever called cantilever to detect and record the surface morphology of the sample. Tip-cantilever assay, called a probe, depending on the operating mode, interacts with the sample surface. By scanning the surface, interaction causes the probe to sense the samples' valleys and hills. Laser diode releases a light on the backside of a cantilever, replicating the up and down probe movement. A mirror reflects light motion to a four quadrant position sensitive photodiode (PSPD). Upon receiving light, the PSPD converts the signal to a computer readable voltage. Computer software then interprets a change in voltage as an oscillation in height, thus creating a surface topography in a three-dimensional high-resolution image (Figure 2.C).

The feedback loop is another important part of the AFM that maintains the probe-sample interaction and minimises noise. By controlling the force between the tip and sample and maintaining their interaction constant, the

---

<sup>2</sup> Electrons excited by the voltage tunnel across the gap between the probe tip and the sample surface

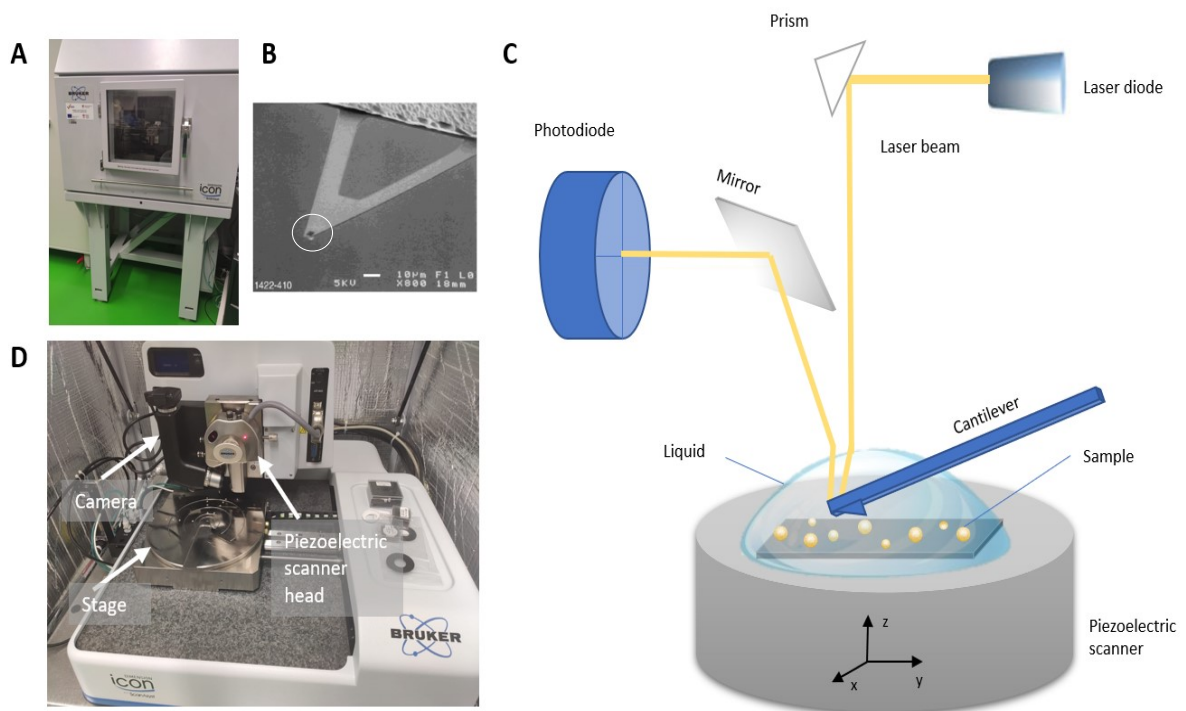


**Figure 2.** Bruker Dimension Icon Scanning Probe Microscope (SPM) - A. outer and D. inner configuration. B. Bruker's SCANASYST-FLUID probe coated with reflective gold, and its tip size (encircled) in regards to triangular cantilever. Scale bar represents 10  $\mu\text{m}$  length [26]. C. Schematic image of AFM principle in liquid imaging. Diode releases a laser beam reflected to the back of the cantilever. The cantilever-tip assay called probe moves up and down, portraying shape of the nanoparticles. The beam is further sent to the photodiode to convert movement changes into computer readable voltage. B. retrieved from [26], C. retrieved and modified from [3].

loop insures 3D image mapping is as close as the original sample surface. Piezoelectric scanner, an element of the loop, is made out of crystal that expands and contracts proportionally to an applied voltage. The scanner can be either mounted on the probe (Figure 2.D) or be a part of the sample holder as illustrated in the Figure 2.C. Every time a probe scans a sample, depending on an operating mode, it either creates a cantilever's deflection<sup>3</sup> or amplitude movement change, reflecting the shape of the surface. The user sets the setpoint<sup>4</sup> value between the tip and the sample and the system compares it to the signals obtained from the PSPD.

<sup>3</sup> Represents the cantilever's bending with respect to the equilibrium position

<sup>4</sup> The setpoint value is a user input that determines the magnitude of the tip-sample interaction.

Voltage signals from the PSPD are converted to the force, and then subtracted from the distance we want to hold constant, a setpoint value. Subtraction of these creates an error signal, a value that is scaled by the control referred to as gain. Setting the gain too low, the feedback loop will respond too slowly to the changes in topography, while the opposite will result in electrical noise coming from interference from the feedback. The gain value controls the piezoelectric scanner movement in z-direction, therefore controlling the distance between the probe and sample support. In such a way, signals received by PSPD equal the sample surface topography to within a minimal error. Since the laser diode can cause mechanical drift of the probe due to heating effect imposed on the piezoelectric scanner [27], heat and vibration protection is ensured by the enclosed system (Figure 2.A) for maintaining the best feedback loop performance.

### 1.3.2 Operating modes

Different operating modes have been developed to encounter sample differences and gain a wide array of information on the examined sample. According to the nature of the tip motion, AFM operation is usually described in one of the three modes. In contact or static mode (CM) (opposed to tapping and non-contact mode as dynamic ones) the tip is in physical contact with the sample surface. Monitoring vertical deflection results in the final image. Beside topography, in case of lateral cantilever motion, CM can provide information on frictional force. Advantages of the mode include high scan speeds, possibility of atomic resolution on flat samples, and scanning rough samples with large changes in vertical topography. Disadvantages include high lateral and capillary forces. Lateral forces imposed by friction, can damage the sample and the tip, while capillary forces from adsorbed liquid can cause high adhesion and thus displace bound particulates. To come around these issues, non-contact mode (NC) was invented. In it, the probe oscillates just above the sample

surface at its resonant frequency<sup>5</sup>, with tip not coming in contact with the sample. When the tip is closer to the sample surface, the probe's amplitude of oscillation decreases along with resonant frequency, and data of these changes produces the final image. Beside topography, NC provides information on phase shift<sup>6</sup>, and amplitude. Advantages include the lowest forces exerted on the surface, no damage to the tip and sample, and bigger prevention of artifacts since the tip does not stick to the surface. Still, only in ultra-high vacuum conditions is the liquid-tip adsorption prevented. Other disadvantages are lower resolution and slower scan speed. To get the best of both modes, Tapping mode and subsequently PeakForce Tapping were invented. Tapping mode (TM) is also referred to as intermittent and vibrant mode. So called, because probe changes its motion intermittently from oscillation across the sample surface to tapping the sample at the lowest position of oscillation. Measured is the change in amplitude, and the amplitude typically serves as the feedback signal for imaging the sample surface. The oscillation is both greater than in non-contact mode, making easier for the loop to create a better resolution, and reduced in contact time between the sample and the probe, thereby protecting the sample structure. Beside topography and amplitude, TM also provides information on phase change. Although TM offers substantial benefits over contact and non-contact mode, especially for studying biological samples, the latest mode improvements came from Bruker's PeakForce Tapping® mode (PFT) (Bruker Corporation, MA, USA) introduced in 2009. Technology focused on TM's most prevalent shortcomings: TM restricts the amount of information obtained from sample, the feedback loop is often unstable because of the constant vibration amplitude, tapping dynamics depends on sample properties and in comparison to CM it offers low-resolution images. To compensate for feedback instability, PFT is operating in a non-resonant mode, performed at frequencies well below the

---

<sup>5</sup> Spontaneous natural frequency at which a system tends to oscillate due to thermal and Brownian particle motion

<sup>6</sup> The phase shift is a change in the frequency of the tip's oscillation during the interaction between the tip and surface, causing the oscillation to lag.

cantilever resonance, thus avoiding dynamics of a resonating system. Similar to TM, lateral and shear forces are negligible due to short interaction time, but measured are the force curves, through which the feedback algorithm recognises the local peak force and triggers the z-piezo to retract. Operating below the baseline setpoint (trigger force) allows operation at forces minimised to a few tens of pico Newton, crucial for obtaining high-resolution data on soft samples. Using PFT, user can collect additional information on adhesion, deformation, elastic modulus and sample dissipation, among others [8,28,29].

### 1.3.3 Probe selection for investigating biofluids in tapping mode

The force needed to extend or compress a spring by some distance is proportional to that distance. That is a principle of Hooke's law:

$$F = -kx \quad (1)$$

whereas  $F$  [N] is a force applied to the spring,  $k$  [N/m] is a spring constant, and  $x$  [m] is a displacement of the spring. Hooke's law provided a cornerstone for many devices over the centuries, including an AFM probe itself. Comprised of a sharp tip and a microcantilever, a typical AFM probe (also called a spring) plays the role of a force transducer. The interaction force between the tip and sample deflects the cantilever. Converting a small force  $F$  into a large displacement  $x$ , requires a small spring constant  $k$  or, in other words, higher sensitivity requires cantilever's softness. Together with force sensitivity, robustness against environmental disturbances should be considered. This is accomplished by setting a resonance frequency. Specifically looking at a TM in the liquid environment, vibrational disturbances are high, and can exceed the cantilever's natural frequency of vibration causing artificial signal [30]. Therefore, to ensure both probe stability in a wide dynamic frequency range, and a sensitivity without damage, resonant frequencies for soft biological samples in TM are in the range 50-150 kHz, and a spring constant that governs cantilever's stiffness around  $k = 0.3-1$  N/m. Probes are usually made out of silicon or silicon

nitride. Silicon probes can be made sharper and possess good manufacturability, and silicon nitride probes can be made thinner, should wear less, and are thus reserved for softer cantilevers with lower spring constants. Thereby, to couple the merits of both materials, hybrid AFM probes are usually constructed [31]. As for example, hybrid probes can be constructed of a nitride cantilever and a silicon tip. Liquid environment provides imaging samples in their native condition, especially relevant for biological samples, like EVs. In addition, when scanned under the fluid conditions, surface tension is eliminated from the adsorbed fluid layer on the tip. Still, liquid imaging provides its own challenges, like refractive index that alters the laser path. Using a camera, the user sets a laser light on the backside of the cantilever (Figure 2.C and D). When the beam is released onto the back of the cantilever head, it is subjected to light refraction in liquid. Refraction occurs not only in the water, but it also happens when the laser beam reflects from the cantilever holder to the mirror. In such refractions, laser light can be easily displaced out of focus. To encounter such issues, manufacturer advises first aligning cantilever in the air, and then realigning it in liquid, as well as optimising scan parameters like rate, setpoint and gains [26]. Additionally, to ensure better reflection, probes for the scan in liquid are coated with reflective material like gold (Figure 2.B).

#### **1.4 TRPS and AFM techniques in EV characterisation**

Improving the knowledge of nanotechnology can help address medical conditions more widely. TBI is a life-threatening intracranial lesion affecting 64 to 74 million people worldwide each year [32]. The rate of recovery of the central nervous system depends on the plasticity and rate of re-establishment of synaptic connections [33]. Along with other roles, EV role as a potential mediator in the intercellular communication of neurons and glial cells after brain injury has been investigated [34]. The most researched EV subgroup, exosomes (50-200 nm), in animal models have been shown to stimulate neuroplasticity and reduce long term

neuroinflammation [35]. Although EVs from human plasma were successfully isolated after TBI, studies on cerebrospinal fluid (CSF) are limited due to the sample volume, and medical and ethical reasons of sample collection. Nonetheless, CSF is not high in particle concentration ( $10^8$  particles/mL), in comparison with other biofluids, like blood ( $10^{12}$  particles/mL) [36]. Kuharic et al. showed that the physical characteristics and protein composition of EVs in the CSF change in response to injury [4]. It was observed that the first 7 days after severe TBI vesicles change their protein content, size, and concentration. Before any downstream investigations, such changes need quantification using nanotechnologies that combine different principles - quantification using light scattering or impedance-based techniques like NTA and TRPS, and visualisation using electron or probe microscopical techniques like EM and AFM.

The application of various techniques for EV characterisation brought a lack of standardised methods in literature for a comprehensive presentation of their properties [7]. To address the challenge, in 2018, the International Society for Extracellular Vesicles published recommendations for the use of high-resolution methods in combination with the measurement of EV size and concentration [37]. From that perspective, and taking into account advantages and disadvantages of other techniques discussed earlier (section 1.1), in this study compared is a relatively novel technique using multi-parameter analysis in real-time, TRPS, and a well-established, high resolution characterisation by direct imaging, AFM. Recent reviews as methods of choice for extracellular vesicle research include both TRPS and AFM techniques [7,38]. Both methods provide the advantages of their own, and no single technology has been reported to be inclusive enough to cover the wide spectrum of EV properties independently. Opposite to electron microscopy, AFM and TRPS are techniques not limited by optical diffraction limit, able to collect data on EVs in their natural environment in a more time and sample efficient way, offering much simpler sample preparation protocols. Moreover, both methods use micrometric sample volumes (TRPS



35  $\mu\text{L}$  and AFM  $\leq 100 \mu\text{L}$ ) important for biofluids like CSF that are limited in collection volume. TRPS greatest advantage is the ability to count NPs simultaneously, with a software instructions leading the user through the measurement protocol. Unlike other techniques that usually report "total" concentration, TRPS provides information on a concentration range over a defined (nanopore) size range, thus improving comparability across laboratories [21]. Although recommended measurement particle count around 500 [13] is difficult to reach without prior user experience on qNano devices, when reached, they can distinct different particle subgroups. Additional parameters like zeta potential calculation can also be useful to serve as an indicator of colloidal stability and their tendency to aggregate, [39] the process in which NPs size misrepresentation can occur. On the other hand, though native AFM imaging in liquid holds its challenges, it provides relatively undeteriorated vesicles, with maximally preserved shape. Protein concentration in CSF, 100 times lower than in blood [40], enables obtaining clear native EV sample image, without prior EV isolation. EVs spontaneously attach to atomically flat surface (mica) [41], maximally simplifying protocol. Besides sample handling kept to minimum, AFM provides detailed morphological information, and data are easily processed to obtain particle size distribution after imaging.

## 2. The goal

The aim of this study was to compare quantitative data obtained from the TRPS measurements with AFM images of NPs in CSF.

The specific objectives of the thesis were:

- 1) to determine the optimal protocol for TRPS measurement of concentration and size distribution for NPs in CSF
- 2) to establish sample preparation protocol for measurement of size distribution of NPs in CSF by AFM in liquid
- 3) to implement image processing modifications of AFM figures in a non-destructive way
- 4) to compare the nanoparticle size distribution in both methods using a statistical test
- 5) to approximate concentration of NPs in AFM measurement

### 3. Materials and methods

#### 3.1 Sample collection

Samples were available from the CSF biobank at Medical faculty in Rijeka. Since sample collection was not a part of the master's thesis, the following description will provide only basic information. The CSF samples were collected from a patient in the early days after severe TBI at the Clinical Hospital Centre Rijeka, Rijeka, Croatia. Sample collection was performed by ventriculostomy<sup>7</sup>. Informed consent was obtained from a family member. The study was conducted according to the guidelines of the Declaration of Helsinki, and approved by the Ethics Committee at Clinical Hospital Centre Rijeka, Rijeka, Croatia (Class: 003-05/19-1/57, Reg. number: 2170-29-02/1-19-2, 7 May 2019).

#### 3.2 Tunable Resistive Pulse Sensing

##### 3.2.1 Chemicals and reagents

TRPS Reagent kit was bought from Izon Science Ltd. The kit contains 1x wetting solution concentrate, 1x - 8.5 g coating solution (CS), 4x - PBS tablets. 20x - 13 mm x 0.22 µm syringe filter, 4x - 25 mm x 0.45 µm syringe filter, and 1x - Reagent kit technical note. All solutions were prepared according to the manufacturer's instructions [42]. Also purchased from the same manufacturer were two different size ranged nanopores, NP80 and NP100, with the detection of 40-255 nm and 50-330 nm, respectively.

##### 3.2.2 Polystyrene standards

Carboxyl Polystyrene Particle Standards denoted as calibration particles, CPC100, were also purchased from Izon Science Ltd. CPC100 have a mean nominal diameter of 100 nm, and a target concentration of  $10^{10}$

---

<sup>7</sup> A surgical process of cerebrospinal fluid drainage from the brain's ventricles to an external collecting device

particles/mL [13]. They were used as a reference in size and concentration calibration.

### 3.2.3 Solution and sample preparation

A batch of measurement electrolyte (ME) was prepared from one PBS tablet dissolved in 200 mL of deionized water (DI). 600  $\mu$ L of wetting solution concentrate was added to the PBS solution, and left to gently swirl on a magnetic stirrer. Wetting solution (WS) was prepared from 9.9 mL of 25% ethanol (Gram-Mol, Croatia)/ME solution and 100  $\mu$ L of wetting solution concentrate. CS was prepared adding 2 grams of the CS powder to the 15 mL of ME warmed in a water bath. The solution was mixed until clear, and topped up with ME to make a total of 20 mL. Before measurements, solution aliquots of ME and WS were filtered with a 0.22  $\mu$ m, and CS with a 0.45  $\mu$ m filter. Fresh stock solutions were prepared weekly, and stored on +4 °C in between the measurements. To work on the qNano Gold device, native CSF sample was filtered with 0.2  $\mu$ m filter and pre-diluted with ME (1:1, 1:10, and 1:20). Prior to analysis, the sample was vortexed for 30 seconds.

### 3.2.4 Instrument settings and analysis

All measurements were performed using a qNano Gold device with associated data collection and analysis software, Izon Control Suite V3.2. (Izon Science Ltd, Christchurch, New Zealand). Steps for concentration and size measurement in biological sample were performed as follows. Within the program, entered was nanopore data, data on samples and calibration particles. Selected was the desired observed particle size range. Afterwards, fluid cell preparation followed. Precleaning step was done always before the change of fluid, and consisted of washing the upper chamber with DI, and drying it with lint-free wipes. 75  $\mu$ L 70% ethanol was added to the lower chamber, and replaced after 30 s with 75  $\mu$ L ME. From lower chamber was removed ME, while remaining moist.

Nanopore was placed on the device and stretched to 47.00 mm. Humidification protocol consisted of adding 75  $\mu\text{L}$  WS to the lower chamber, precleaning the upper chamber and adding 35  $\mu\text{L}$  WS, closing the fluid cell, and applying maximum pressure (20 mbar) for 2 minutes. Coating protocol followed the same precleaning steps, with placing the nanopore on the crucifex, adding 75  $\mu\text{L}$  of CS to the lower chamber, and adding 35  $\mu\text{L}$  of CS in the upper chamber. Maximum pressure was applied for 10 min. Next, nanopore was re-equilibrated with ME. Then, calibration followed. After precleaning protocol, 35  $\mu\text{L}$  of the calibration particle solution was added to the upper chamber, nanopore elongation was optimised, two pressures selected and data were recorded. Measurement of concentration and particle size distribution in the sample was done in a similar manner without changing the stretch or pressures. After calibration, the protocol was repeated for the same CSF sample in three different dilutions: 2x, 11x, and 21x, in different pressures (NP80 – 9 and 4 mbar, NP100 – 8 and 4 mbar) and using two different size range nanopores, NP80 and NP100, according to manufacturer's recommendations (4). Accordingly, stretch and voltage were set to 45.05 mm ; 1.18 V on NP80, and 45.86 mm ; 0.88 V on NP100. Recording time was 120 seconds.

### **3.3 Atomic Force Microscopy**

AFM analysis was performed in a tapping mode in liquid on a Dimension Icon SPM (Bruker Corporation, MA, USA). A 80  $\mu\text{L}$  of the native CSF sample, filtered over 0.2  $\mu\text{m}$  filter, was pipetted directly on freshly cleaved mica, and left 10-15 minutes for particles to settle down. To avoid capillary forces from the probe's contact with the sample fluid, additional 10  $\mu\text{L}$  of the sample was placed onto the cantilever's tip. A larger overview image of 5x5  $\mu\text{m}$  was first made, after which the area rich in NPs was recognised (1x1  $\mu\text{m}$ ) and selected for the complete scan. The image needs to be obtained relatively quickly due to the evaporation

rate of the native sample (within 45 minutes). Images were obtained using a silicon nitride SCANASYST-FLUID probes (Bruker Corporation, MA, USA). Probe nominal tip radius is 20 nm, resonant frequency 150 kHz, and a spring constant 0.9 N/m. Scan rate was 0.797 Hz, Peak Force Amplitude 70 nm, and a resolution 512 dots per pixel. Two different software programs were employed for particle analysis: Gwyddion 2.56 (Czech Metrology Institute, Czech Republic) and NanoScope analysis 1.50 (Bruker Corporation, MA, USA) image visualisation and analysis tools.

### 3.3.1 NanoScope Analysis

NanoScope Analysis 1.50 software was used to process raw image after AFM scanning. Firstly, to remove image tilt, bow and to fit each line individually to center the data, performed was *Flatten command*, 3<sup>rd</sup> order. Secondly, to distinguish NPs from the background, *Plain fit* 0<sup>th</sup> order was applied to center the data (0<sup>th</sup> order) around the chosen part that was visually particle free. Then, particle count was done in Gwyddion.

### 3.3.2 Gwyddion

Gwyddion 2.56, open source software for visualisation and analysis of data obtained by scanning probe microscopy techniques [43], was used for precise nanoparticle marking. *Stretch color range* option was used to include the nanoparticle data. *Mark grains by threshold* was applied to visually mark NPs. To obtain more clear image, i.e. nanoparticle count, and remove particle artifacts, *Edit mask* option was utilized for removal of dots that were either too small or not round. Only diameter from whole NPs that had clear boundaries (were not on the edge) from 10 1x1  $\mu\text{m}$  images was used to obtain particle size distribution. *Grain Distributions* were used to export raw data of Maximum Martin diameter<sup>8</sup> plotted against

---

<sup>8</sup> The Martin's diameter is described as the length of line through the grain which divides the grain area into two equal parts (median line).

particle count to Microsoft Excel for further analysis. *Data Process – Grains – Summary* provided useful integrative grain data on parameters such as grain number, total projected area, mean grain area, size, and volume. Additional scar removal option *Correct horizontal strokes* was applied to images before saving in .tiff format.

### 3.3.3 Concentration approximation

To approximate the number of NPs detected by AFM, the following formula was used:

$$\text{EV concentration (particles/mL)} = \left( \frac{\text{conversion factor from 1 } \mu\text{L to 1 mL}}{\text{pipetted volume of CSF sample}} \right) \times \left( \frac{\text{surface area of the mica}}{\text{surface area of an AFM image}} \right) \times N_{\text{AFM}} \quad (2)$$

$$\text{EV concentration (particles/mL)} = \left( \frac{10^3}{80 \mu\text{L}} \right) \times \left( 78.5 \times \frac{10^6 \mu\text{m}^2}{1 \mu\text{m}^2} \right) \times 17, \quad (2a)$$

where  $10^3$  is the conversion factor from  $\mu\text{L}$  to 1 mL, 80  $\mu\text{L}$  is the pipetted volume of the CSF sample applied to the mica surface,  $78.5 \times 10^6 \mu\text{m}^2$  is the surface area of the mica calculated from the surface of a circle,  $A = \pi r^2$ , where mica's radius is  $r = 5 \text{ mm}$ .  $1 \mu\text{m}^2$  is the surface area of an AFM image, and  $N_{\text{AFM}}$  is the mean of the total number of NPs per image [8,44].

## 3.4 Statistical analysis

Statistical analysis was performed in Microsoft Excel software version 2107 (Microsoft Corporation, WA, USA). Data distribution was downloaded in .csv format from both Gwyddion and Izon Control Suite softwares, and tested using Data Analysis Toolpack. The distribution was tested using Kolmogorov-Smirnov test and was approximately normal. Parametric two sample t-Test assuming unequal variances followed. Alpha value was set to 0.05.  $H_0$  was hypothesized as 0 nm in mean difference. A difference at  $p \leq 0.05$  was considered significant.

## 4. Results

### **4.1 Tunable resistive pulse sensing measurements with NP80 and NP100 nanopore of cerebrospinal fluid**

The first experiment was to compare both NP80 and NP100 nanopore according to their performance. For this purpose, Table 1. shows the data acquired after recordings from NP80 and NP100 nanopores, respectively. Measurement count of calibration particles was 1018-1152 particles, particle rate of 585.1-1204.9 particles/min, current 84.99-150.39 nA, and RMS noise was 19.88-58.00 pA.

NP80 resulted with measurement count in the range of 22-148 particles, particle rate 8.5-73.9 particles/min, and current 78.22-121.07 nA. For NP100, a particle count range of 4-64 particles, particle rate of 2-27.5 particles/min and current 40.87-150.39 nA were recorded. RMS noise was 12.05-74.88 pA for NP80 and 17.68-24.19 pA for NP100. Concentration across both nanopores was with a detected range of 1.07- $4.74 \times 10^9$  particles/mL. NP100 has not recorded particles below 70 nm, (Table 1.), while NP80 registered 3 particles below 35 nm (11x dilution).



**Table 1.** Nanopore performance data measurement for NP80 and NP100 nanopore using tunable resistive pulse sensing technique. Dilution (2x, 11x, 21x) with belonging mean, concentration, count, average current, average root mean square (RMS) noise and particle rate across two point pressure – 9 and 4mbar for cerebrospinal fluid samples and calibration particles (CPC100).

	Dilution	Mean diameter (nm)	Concentration (particles/mL)	Particle count	Average current (nA)	Average RMS noise (pA)	Particle rate (particles/min)	Pressure (mbar)
NP80	2x	98	$1.07 \times 10^9$	148	85.35	37.38	73.9	9
	11x	60	$1.31 \times 10^9$	45	120.36	12.05	21.5	
	21x	86	$4.74 \times 10^9$	115	114.15	28.87	57.4	
	CPC100 1001x	/	/	1018	84.99	33.73	832.5	
	2x	106	$1.07 \times 10^9$	128	78.22	74.88	63.3	4
	11x	63	$1.31 \times 10^9$	19	120.52	37.99	8.5	
	21x	67	$4.74 \times 10^9$	22	121.07	12.72	10.5	
	CPC100 1001x	/	/	1152	86.47	58.00	585.1	
NP100	2x	114	$2.3 \times 10^9$	40	75.53	20.58	20	8
	11x	114	$1.3 \times 10^9$	15	74.91	18.04	7.5	
	21x	113	$1.9 \times 10^9$	64	40.87	18.90	27.5	
	CPC100 1001x	/	/	1027	150.39	22.00	1204.9	
	2x	112	$2.3 \times 10^9$	4	73.86	24.19	2	4
	11x	110	$1.3 \times 10^9$	13	76.36	17.68	6.5	
	21x	106	$1.9 \times 10^9$	26	40.90	19.70	12.8	
	CPC100 1001x	/	/	1024	147.99	19.88	1014.7	

## **4.2 Stability of tunable resistive pulse sensing measurements for cerebrospinal fluid**

Stability of TRPS measurements for CSF is influenced by sample dilution. To investigate how different dilutions influenced the measurement, the second experiment included creating rate plots. In Figure 3. demonstrated are rate plots of calibration particles (A. and C.), and between different sample pressures (B. and D.) across three dilutions – 2x, 11x and 21x. Calibration particles were visibly more numerous than the sample particles on both nanopores (Figure 3.A example on 9 mbar pressure and C example on 8 bar pressure). Despite 2x and 21x dilutions having mostly higher particle count, they show instability in the rate signal. By contrast, 11x recorded the most stable (linear) rates over both pressures, and on both nanopores with the least pore clogging events (Figure 3.B and D).

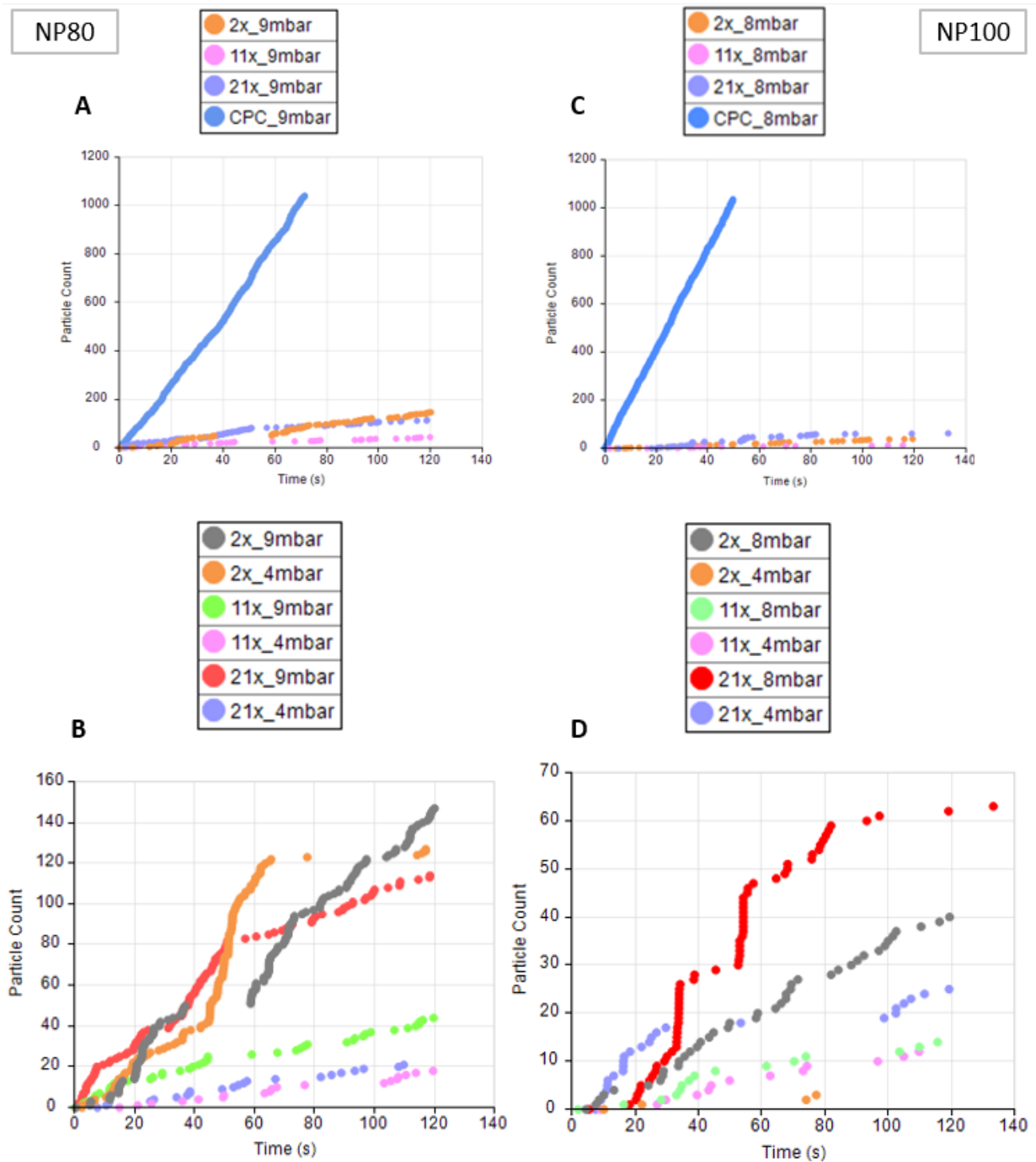


**Figure 3.** Rate plot - particle count versus time for NP80 (A and B) and NP100 measurement (C and D) of cerebrospinal fluid sample. A. and C. three different sample dilutions (2x, 11x, and 21x) in comparison with calibration particles (CPC100) using higher pressure show notably lower count on both nanopores. B. and D. three different sample dilutions compared at higher and lower pressure show the least clogging events on both nanopores, and on both pressures on 11x dilution.

### **4.3 Image processing protocol with representative atomic force microscopy images of cerebrospinal fluid**

After obtaining diameter and concentration from TRPS measurements, the third experiment included setting a protocol for image processing following AFM imaging to obtain size distribution and concentration of NPs in CSF. Ten  $1 \times 1 \text{ }\mu\text{m}^2$  images were cropped from either 5 or 2 micrometer wide images. Representative  $5 \times 1.5 \text{ }\mu\text{m}$  AFM image is presented in Figure 4. For each image *Flatten* and *Plain fit* steps were applied using Nanoscope (Figure 4.A). After that, in Gwyddion, particle marking by threshold was selected in the range between 1 and 3 nm to eliminate most of the background interference [45]. To be sure that all the visible particles were detected by particle marking by threshold, for comparison was used the same image in Nanoscope, but unmarked, and showing topography (Figure 4.B). After that, some NPs have been still left unmarked, the reason why the advanced *Mask Editor* option for manual marking in Gwyddion was used (Figure 4.C). Individual particle removal was used for dust-like particles that were considered noise. On the hypothesis that all NPs adsorb onto the mica surface [8,44], calculated was NP concentration with 17 particles as the average count on 10  $1 \times 1 \text{ }\mu\text{m}^2$  images ( $N_{\text{AFM}}$ ) (section 3.3.3), and it equaled  $1.67 \times 10^{10}$  particles/mL. Round and cup-shape profiles were identified, but not demonstrated since they were not the main objective of the thesis.

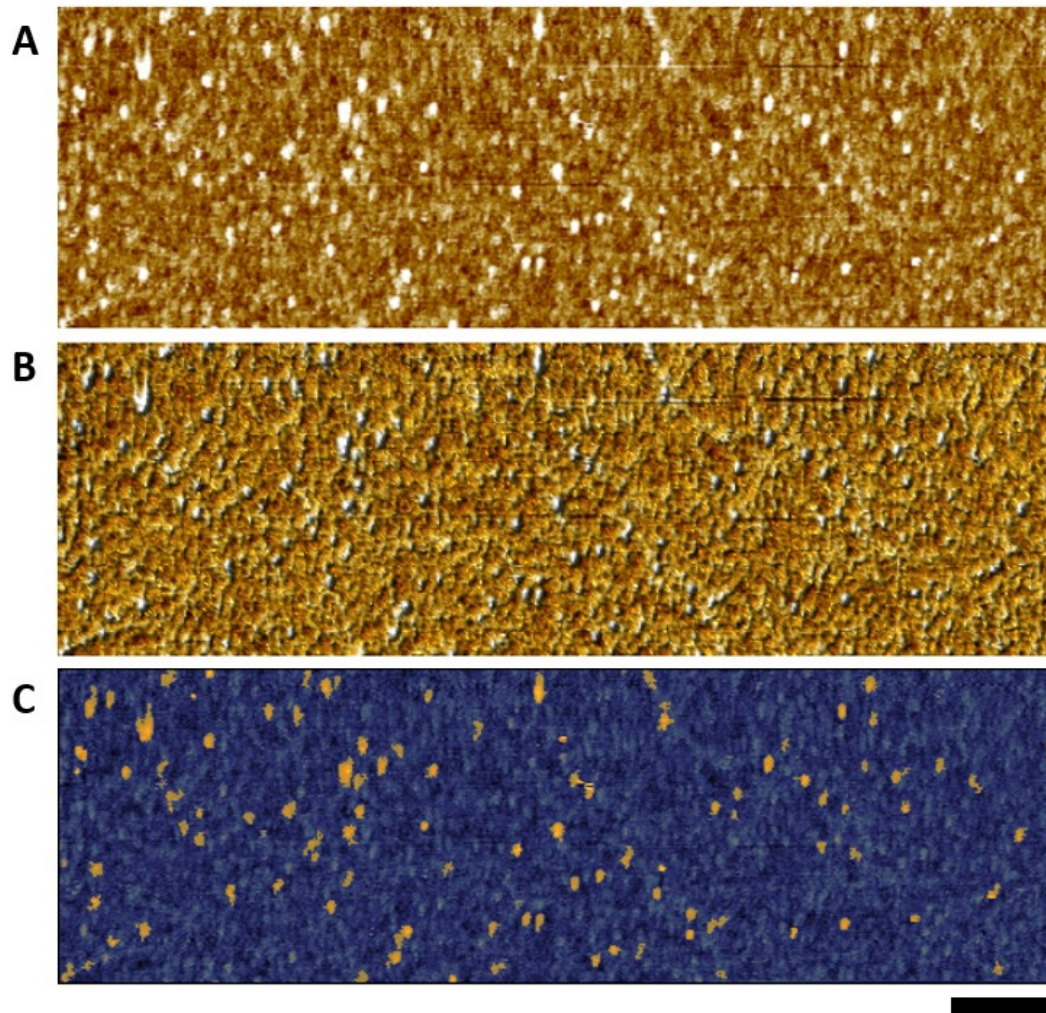


**Figure 4.** Atomic force microscopy topography images performed in tapping mode of nanoparticles analysed from human cerebrospinal fluid in  $5 \times 1.5 \mu\text{m}$  frame processed in different ways. A. flattened and plain fitted, B. planar topography, C. marked particles ( $n=100$ ) detected as features above the threshold of zero. A. and B. processed in Nanoscope, and C. in Gwyddion. Scale bar represents 500 nm length.

#### **4.4 Size distribution of nanoparticles in cerebrospinal fluid obtained after tunable resistive pulse sensing and atomic force microscopy measurements**

In Figure 5. compared is the particle size distribution of the most stable TRPS measurement (NP80, 11x dilution) with the marked particles on AFM images. The 56-75 nm range was the most frequent diameter bin obtained from both techniques. Mean diameter  $\pm$  standard deviation (SD) obtained by TRPS on NP80 11x dilution (added particles from both pressure measurements) was  $64.3 \pm 30.7$  nm ( $n_{\text{TRPS}}=64$ ), and the one obtained by AFM technique, by adding particles from 10  $1 \times 1 \mu\text{m}$  AFM images was  $59.2 \pm 22.1$  nm ( $n_{\text{AFM}}=170$ ). Student t-test revealed no significant difference between two sample means, with two-tail significance level of  $p=0.23$ .  $\leq 35$  and 36-55 nm distribution bins for TRPS measurement contain 3 and 17 particles respectively, with 3 particles being exactly 34.35 nm, and 17 particles exactly 40.25 nm in diameter, which disabled error bars to be calculated (Figure 5.A). In nanoparticle size measurements above 95 nm (bin  $>95$  nm), TRPS has shown greater variability, with SD in the bin of 33.6 nm, whereas AFM had SD value of 8.95 nm. Minimum and maximum diameters in observed populations from both techniques were as follows: 34.35 and 201.25 nm (TRPS) and 14.29 and 123.50 nm (AFM).

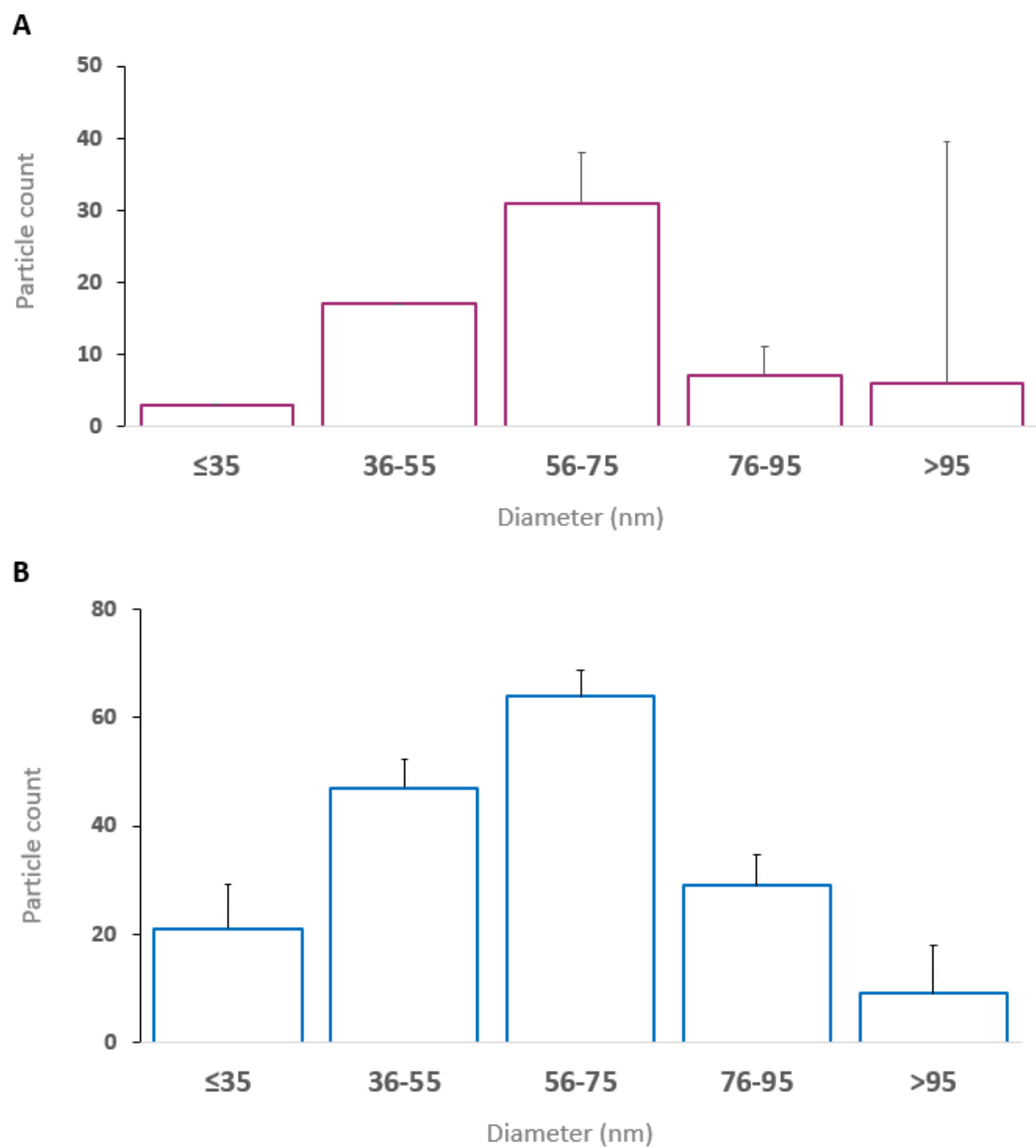


**Figure 5.** A. Nanoparticle size distribution in TRPS measurement on NP80, in 11x dilution, by adding particles from both pressures (4 and 9 mbar). B. Size distribution of randomly selected nanoparticles from 10 1x1  $\mu\text{m}$  AFM images. A. and B. diagrams contain 20 nm bin size between distributions with standard deviation values as box and whisker.

## 5. Discussion

Extracellular vesicles, as intercellular carriers of information, are actively researched as mediators in various pathophysiological conditions, with the opportunity for their translation to clinic [1]. Prior to clinical use, emphasis should be put on obtaining clear quantitative data, like vesicle size distribution and concentration [3]. These data are not only specific for each human biofluid, but also for the examined condition, and the different variables that follow it, like the stage of the disease.

To tackle such issues, standardisation of used protocols and nanotechnologies is required [37]. Based on current knowledge, there are no protocols standardised for AFM imaging in liquid for native CSF samples, and TRPS measurements of CSF sample are also nonexistent. Also, the quantitative data on changes in size and concentration happening after TBI are reported only in several studies before [4,5], but using NTA technique. Therefore, this study describes two advanced techniques in NP detection, TRPS and AFM, and their performance in size distribution and concentration measurement. The initial objective of this study was to investigate the quality of TRPS measurement and to compare the most reliable measurement with the size distribution and concentration obtained through AFM imaging.

To decide what nanopore is more suitable for CSF sample measurement, first experiment compared parameters of measurement condition like particle count, particle rate, average current and RMS noise in both NP80 and NP100 nanopores. The results demonstrated higher particle count, higher particle rate and average current closer to recommended values (110 nA) [16] in nanopore able to detect smaller particles, NP80. RMS noise was overall higher in NP80 than in NP100. This can be due to the higher sensitivity of a smaller nanopore to changes in measurement conditions, that could occur in non-isolated, biological fluids. Even so, lower than recommended values of RMS noise (<15 pA) were obtained only in NP80



measurement, using 11x (9 mbar) and 21x (4 mbar) dilutions. In addition, despite the nanopore size detection range of 50-330, NP100 has not recorded particles below 70nm, while NP80 registered particles below 35nm (11x dilution, 4 mbar, 34.35 nm), despite the nanopore size detection range of 40-255 nm.

Next, second experiment investigated the dilution of native CSF. Examined was serial dilution (2x, 11x, 21x) looking at the stability of rate plots. 11x dilution was found to produce the most linear particle rate during the experiment, with the least pore clogging events and as the dilution that produced the lowest RMS noise value (12.05 pA, recommendation <15 pA) [16]. Still, 11x dilution (NP80) has recorded fairly lower mean diameter (64.3 nm) in comparison to mean diameter from NP100 (111.9 nm). Additionally, in comparison to average calibration particle count ( $n_{CPC100} = 1055$  particles) and recommended lowest number of 200 particles per run [13], particle count added from both measurement pressures in 11x dilution is quite low ( $n_{NP80,11x} = 64$  particles), and questionable in acceptance as a result. Differences in mean diameter between nanopores and the low particle count could have occurred due to several factors. Diameter differences could have been caused by calibration particle standards (CPC100) left remaining after washing steps. As well, less sensitivity for smaller NPs when using larger nanopore, NP100. This is in accordance with the conclusion made by Maas et al. (2015) that EV quantifications can differ between high sensitivity nanopore setups [46], which is here related to the higher mean diameters detected on a larger nanopore, NP100. The low particle count probably occurred due to the nanopore instability (clogging events). Further, nanopore instability could have been influenced by sample preparation protocol since this paper analyzed native biological fluid without the prior isolation step. During the sample collection by ventriculostomy following the TBI, CSF can become contaminated with blood, making the isolation step necessary to distinguish EVs from NPs. For that reason, during the TRPS sample preparation,

surfactant (wetting solution concentrate) is added to reduce the rate of particle aggregation [42]. Surfactant should prevent to a certain extent the adhering of proteins like albumin to nanopores and NPs themselves. It is worth noting that surfactant Tween 20 was used by several different studies when handling EV TRPS measurement [11,20,21]. Since surfactant from wetting solution concentrate was applied as a part of a commercialized reagent kit in this study, it is challenging to comment on its composition and proportion of strength. Therefore, advisable is to try Tween 20 in the next experiments, as it has shown in separate studies to be the least disrupting out of the four detergents analyzed [47], but simultaneously strong enough to provide more stability and higher count when present in the buffer [48]. Moreover, the stronger electrolyte solution (here was used standard electrolyte solution of 1 x PBS tablet) should be used to maximize the ionic space between particles and thus lower the aggregation rate (discussed in section 1.2.2). However, using biological fluid instead of isolated EVs surely influenced the clogging events, in spite of CSF being relatively clean biofluid, with lower protein and particle concentration in comparison to other biofluids like blood [36], discussed previously (section 1.4).

Third experiment followed after AFM imaging, and consisted of setting a protocol to process size distribution and concentration results in a non-destructive manner. AFM data was centered (*Flatten command*) along with removing noise to distinguish the particles from image background (*Plain fit command*). NPs were picked manually with particle marking using mask, allowing higher diameter sensitivity in comparison to TRPS diameter numbers. From the average count on 10 1x1  $\mu\text{m}^2$  images, concentration approximation was calculated.

In the fourth experiment compared were particle size distributions from both techniques. In 36-55 and 76-95 nm bin ranges, AFM had an increased number of particles in relation to TRPS. As a result, AFM distribution was

closer to normal, Gaussian distribution. Moreover, AFM distribution had less variation around the mean, demonstrated especially for the upper (>95 nm) size-ranged NPs. High SD value for TRPS is related to previously discussed nanopore instability, whereas AFM detected lower SD value due to increased sensitivity introduced by manual marking step in image post-processing. Furthermore, Control Suite software had evident discrepancy in detecting lower ranges ( $\leq 35$  and 36-55 nm bins) due to the nanopore size limit (around 30 nm in general for qNano Gold measurements). It resulted in detection of NPs of the same size (no SD value) in the bins. Particle size distribution comparison confirmed the biggest particle distribution in the 56-75 nm range, with AFM demonstrating approximated concentration one fold higher than TRPS,  $1.7 \times 10^{10}$  particles/mL in comparison with  $1.3 \times 10^9$  particles/mL (NP80, 11x dilution).

Although multiple studies observed EV diameter and concentration in cell cultures, data about native, human CSF measurement after TBI was found only in two papers. In the first study, Kuharic et al (2019) used NTA technique to compare the change in diameter and concentration of EVs isolated by ultracentrifugation, from the control group and TBI patients. Hypothesized was that intracranial EV size and volume change in the shedding process as a neuroprotection response in the early phase after a severe TBI. Researchers reported on enlarged intracranial EVs on the day 4 – 7 ( $205 \pm 40$  nm) in contrast with EV size in the early days of TBI (day 2 – 3:  $141 \pm 41$  nm), (control:  $157 \pm 24$  nm)[4]. Along with increased EV diameter, two different concentration groups -  $4.58 \times 10^8$  and  $3.66 \times 10^{10}$  particles/mL were detected. Patients with a favorable outcome had EV concentrations comparable to controls ( $4.29 \times 10^8$  particles/mL), while patients with an unfavorable outcome tended to have an increased EV concentration in comparison to the control group [4]. In a second study, Manek et al (2018) also used EVs isolated by ultracentrifugation, and the same NTA technique. Researchers reported concentration range of  $27.8 - 33.6 \times 10^8$  particles/mL, and a slight increase in concentration in

comparison to control ( $13.1 - 18.5 \times 10^8$  particles/mL) [5]. Concentration reported in the thesis was in the upper range ( $10^9$  and  $10^{10}$ ) of reported numbers from Kuharic et al, and higher than what Manek et al reported. Since the AFM concentration formula was approximated, and changed from the original paper [44], it should be confirmed by additional experiments. In contrast to the above study [4] where slightly larger diameters were reported, diameter range reported from Manek et al was closer to the one reported in this study, 74-98 nm [5]. However, both researchers used NanoSight NS300 in their NTA analysis that in a separate study [49] failed to report a peak EV diameter below 60 nm which could have skewed their quantitative results. Interestingly, Akers et al. (2016) isolated EVs using differential centrifugation from CSF in glioblastoma patients and compared the sample in four different techniques: TRPS, NTA, transmission electron microscopy (TEM) and vesicle flow cytometry (VFC). NTA detected more EVs than TRPS for EVs <150 nm in diameter, while TRPS detected more EVs than NTA for EVs >150nm diameter. However, nanopores that authors used in TRPS measurement were NP200, NP300 and NP1000 [50]. The minimum detectable vesicle size for NP200 is ~80 nm, for NP300 ~150 nm, and for NP1000 ~490 nm [13], the usage of which probably prevented the authors to detect bigger count of smaller EVs using TRPS. One more reason that supports why researchers detected more larger EVs is that their EV sample was 0.8  $\mu\text{m}$  filtered, while here was 0.2  $\mu\text{m}$  filtered. In other studies researchers also used smaller filters, mostly 0.2  $\mu\text{m}$  [4,11,46], or maximally 0.45  $\mu\text{m}$  [5,18], to remove cell debris or larger vesicles, like apoptotic bodies.

Lower particle diameter distribution reported in the thesis (56-75nm, result section 4.4) could be explained by the particle-by-particle analysis obtained through TRPS nanopore stretching sensitivity, usage of a nanopore with the lowest detection range available (NP80, range 40-255 nm), and manual masking in AFM. Yet, concentration obtained with AFM was formula-approximated, and TRPS measurements were rather unstable in rate and

low in particle count, indicating of problems like nanopore clogging. Future TRPS measurements should be further optimised to reach more stable conditions and overall higher particle number. For this particular sample, calibration particle standards, CPC70, with a nominal diameter of 70 nm should be used along with the larger ones used in this study (CPC100). AFM measurements should include more analyzed particles (pictures). To prevent soluble proteins and/or NPs to potentially aggregate, using a stronger electrolyte solution coupled with Tween 20 surfactant could be an option in future experiments. When a high count is reached in TRPS measurement (1000 events per run), it can differentiate the EV subgroups by their size distribution [11]. What is more, a suitable isolation method should precede measurement of both techniques. As an example, to distinguish if all observed NPs are of vesicle origin, immunocapture/labelling technique could be used prior to TRPS, and tip-antibody functionalisation prior to AFM imaging. The results of native CSF presented in the thesis provide initial quantitative data of NPs in the TBI affected biofluid. They also indicate of further experiments needed to examine what caused the instability problems in TRPS measurement. On one hand, isolation could have improved TRPS measurement conditions, but on the other hand, it could have made it even harder to get the particle count of couple hundred particles per run. What is more, AFM image has shown relatively clear NPs. AFM visualisation confirmed previous findings that electrostatic interaction between the bare surface of mica and the EVs is sufficient to keep them attached to the surface [41].

Coupling these methods can provide insight into a wide range of EV subgroup sizes. TRPS can provide information on polydispersity by quantifying 30 nm to 1  $\mu$ m NP size range, while AFM can bridge the gap to identify smaller NPs (<30 nm). Stability in TRPS could be improved by sample prefiltration/isolation and usage of different sized nanopores (NP80 – NP400) for obtaining a wide range of NP distribution, and in AFM by testing a non-resonant, PFT mode.

## 6. Conclusion

TRPS and AFM methods were found suitable for characterisation of native CSF. Both TRPS and AFM resulted in similar NP diameter of around 60 nm. Concentration was one fold lower in TRPS than in AFM. In TRPS, setting the parameters for more stable and high-throughput measurement should be a priority, while for AFM, a concentration approximation needs to be further validated. TRPS brought a quantitative advantage in a simultaneous measurement of NP size and concentration, while AFM provided comparable data and NP visualisation.

Both methods enable measurement of EVs in their native condition, use noncomplex sample preparation protocols, and need a low amount of sample volume for analysis.

Altogether, a comparison of the TRPS and AFM technique provides a preliminary information for future EV characterisation technique investigations.

Since both TRPS and AFM are relatively novel methods in EV research, further research on the isolation and optimisation of method protocols are needed. In the future, nanotechnologies can be coupled with isolation methods like immunodetection that can help differentiate between specific EV subgroups for more accessible utilization in EV-related theranostics.

## 7. Bibliography

1. Soekmadji, C.; Li, B.; Huang, Y.; Wang, H.; An, T.; Liu, C.; Pan, W.; Chen, J.; Cheung, L.; Falcon-Perez, J.M.; et al. The Future of Extracellular Vesicles as Theranostics - an ISEV Meeting Report. *J Extracell Vesicles* **2020**, *9*, 1809766, doi:10.1080/20013078.2020.1809766.
2. Doyle, L.M.; Wang, M.Z. Overview of Extracellular Vesicles, Their Origin, Composition, Purpose, and Methods for Exosome Isolation and Analysis. *Cells* **2019**, *8*, doi:10.3390/cells8070727.
3. Malenica, M.; Vukomanović, M.; Kurtjak, M.; Masciotti, V.; dal Zilio, S.; Greco, S.; Lazzarino, M.; Krušić, V.; Perčić, M.; Jelovica Badovinac, I.; et al. Perspectives of Microscopy Methods for Morphology Characterisation of Extracellular Vesicles from Human Biofluids. *Biomedicines* **2021**, *9*, 603, doi:10.3390/biomedicines9060603.
4. Kuharić, J.; Grabušić, K.; Tokmadžić, V.S.; Štifter, S.; Tulić, K.; Shevchuk, O.; Lučin, P.; Šustić, A. Severe Traumatic Brain Injury Induces Early Changes in the Physical Properties and Protein Composition of Intracranial Extracellular Vesicles. *J Neurotrauma* **2019**, *36*, 190–200, doi:10.1089/neu.2017.5515.
5. Manek, R.; Moghieb, A.; Yang, Z.; Kumar, D.; Kobessiy, F.; Sarkis, G.A.; Raghavan, V.; Wang, K.K.W. Protein Biomarkers and Neuroproteomics Characterization of Microvesicles/Exosomes from Human Cerebrospinal Fluid Following Traumatic Brain Injury. *Mol Neurobiol* **2018**, *55*, 6112–6128, doi:10.1007/s12035-017-0821-y.
6. Chuo, S.T.-Y.; Chien, J.C.-Y.; Lai, C.P.-K. Imaging Extracellular Vesicles: Current and Emerging Methods. *Journal of Biomedical Science* **2018**, *25*, 91, doi:10.1186/s12929-018-0494-5.
7. Sahoo, S.; Adamiak, M.; Mathiyalagan, P.; Kenneweg, F.; Kafert-Kasting, S.; Thum, T. Therapeutic and Diagnostic Translation of Extracellular Vesicles in Cardiovascular Diseases: Roadmap to the Clinic. *Circulation* **2021**, *143*, 1426–1449, doi:10.1161/CIRCULATIONAHA.120.049254.
8. Hardij, J.; Cecchet, F.; Berquand, A.; Gheldof, D.; Chatelain, C.; Mullier, F.; Chatelain, B.; Dogné, J.-M. Characterisation of Tissue Factor-Bearing Extracellular Vesicles with AFM: Comparison of Air-Tapping-Mode AFM and Liquid Peak Force AFM. *Journal of Extracellular Vesicles* **2013**, *2*, 21045, doi:10.3402/jev.v2i0.21045.
9. Sinha Ray, S. 3 - Structure and Morphology Characterization Techniques. In *Clay-Containing Polymer Nanocomposites*; Sinha Ray, S., Ed.; Elsevier: Amsterdam, 2013; pp. 39–66 ISBN 978-0-444-59437-2.
10. Large-Sample AFM | Large-Stage AFM | Wafer AFM Available online: <https://afm.oxinst.com/products/jupiter-family-of-afms/jupiter-xr-afm> (accessed on 2 June 2021).
11. Vogel, R.; Savage, J.; Muzard, J.; Camera, G.D.; Vella, G.; Law, A.; Marchioni, M.; Mehn, D.; Geiss, O.; Peacock, B.; et al. Measuring Particle Concentration of Multimodal Synthetic Reference Materials and Extracellular Vesicles with Orthogonal Techniques: Who Is up to the Challenge? *Journal of Extracellular Vesicles* **2021**, *10*, e12052, doi:https://doi.org/10.1002/jev2.12052.
12. What Is the Difference between NTA and TRPS? Available online: <https://www.izon.com/trps/compare-nta-and-trps> (accessed on 3 June 2021).
13. QNano Gold User Guide | Izon Science.
14. Graham, M. THE COULTER PRINCIPLE: FOR THE GOOD OF HUMANKIND. *Theses and Dissertations--History* **2020**, doi:https://doi.org/10.13023/etd.2020.495.
15. Willmott, G.R.; Vogel, R.; Yu, S.S.C.; Groenewegen, L.G.; Roberts, G.S.; Kozak, D.; Anderson, W.; Trau, M. Use of Tunable Nanopore Blockade Rates to Investigate Colloidal Dispersions. *J. Phys.: Condens. Matter* **2010**, *22*, 454116, doi:10.1088/0953-8984/22/45/454116.
16. QNano Gold TRPS Measurement | Izon Science Available online: <https://www.izon.com/trps/qnano-gold> (accessed on 6 May 2021).
17. Vogel, R.; Willmott, G.; Kozak, D.; Roberts, G.S.; Anderson, W.; Groenewegen, L.; Glossop, B.; Barnett, A.; Turner, A.; Trau, M. Quantitative Sizing of

- Nano/Microparticles with a Tunable Elastomeric Pore Sensor. *Anal Chem* **2011**, *83*, 3499–3506, doi:10.1021/ac200195n.
18. Coumans, F.A.W.; van der Pol, E.; Böing, A.N.; Hajji, N.; Sturk, G.; van Leeuwen, T.G.; Nieuwland, R. Reproducible Extracellular Vesicle Size and Concentration Determination with Tunable Resistive Pulse Sensing. *J Extracell Vesicles* **2014**, *3*, 25922, doi:10.3402/jev.v3.25922.
  19. Maas, S.L.N.; Vrij, J.D.; Broekman, M.L.D. Quantification and Size-Profiling of Extracellular Vesicles Using Tunable Resistive Pulse Sensing. *JoVE (Journal of Visualized Experiments)* **2014**, e51623, doi:10.3791/51623.
  20. Kozak, D.; Anderson, W.; Vogel, R.; Chen, S.; Antaw, F.; Trau, M. Simultaneous Size and  $\zeta$ -Potential Measurements of Individual Nanoparticles in Dispersion Using Size-Tunable Pore Sensors. *ACS Nano* **2012**, *6*, 6990–6997, doi:10.1021/nn3020322.
  21. Vogel, R.; Coumans, F.A.W.; Maltesen, R.G.; Böing, A.N.; Bonnington, K.E.; Broekman, M.L.; Broom, M.F.; Buzás, E.I.; Christiansen, G.; Hajji, N.; et al. A Standardized Method to Determine the Concentration of Extracellular Vesicles Using Tunable Resistive Pulse Sensing. *J Extracell Vesicles* **2016**, *5*, 31242, doi:10.3402/jev.v5.31242.
  22. Binnig, G.; Quate, C.F.; Gerber, Ch. Atomic Force Microscope. *Phys. Rev. Lett.* **1986**, *56*, 930–933, doi:10.1103/PhysRevLett.56.930.
  23. Mironov, V.L. *Fundamentals of the Scanning Probe Microscopy*; Russian Academy of Sciences, Institute of Physics of Microstructures: Nizhniy Novgorod, 2004;
  24. Fuchs, H.; Hölscher, H.; Schirmeisen, A. Scanning Probe Microscopy. In *Encyclopedia of Materials: Science and Technology*; Buschow, K.H.J., Cahn, R.W., Flemings, M.C., Ilshner, B., Kramer, E.J., Mahajan, S., Veyssi re, P., Eds.; Elsevier: Oxford, 2005; pp. 1–12 ISBN 978-0-08-043152-9.
  25. Hansma, P.K.; Elings, V.B.; Marti, O.; Bracker, C.E. Scanning Tunneling Microscopy and Atomic Force Microscopy: Application to Biology and Technology. *Science* **1988**, *242*, 209–216, doi:10.1126/science.3051380.
  26. Veeco Instruments Inc Icon Service Training: Imaging in Fluid - MMRC 2009.
  27. Molenaar, R.; Prangma, J.C.; van der Werf, K.O.; Bennink, M.L.; Blum, C.; Subramaniam, V. Microcantilever Based Distance Control between a Probe and a Surface. *Review of Scientific Instruments* **2015**, *86*, 063706, doi:10.1063/1.4922885.
  28. Bruker Nano Surfaces Division Introduction to Bruker’s ScanAsyst and PeakForce Tapping AFM Technology.
  29. Sharma, S.; LeClaire, M.; Gimzewski, J.K. Ascent of Atomic Force Microscopy as a Nanoanalytical Tool for Exosomes and Other Extracellular Vesicles. *Nanotechnology* **2018**, *29*, 132001, doi:10.1088/1361-6528/aaab06.
  30. Fukuzawa, K. AFM Probes. In *Encyclopedia of Nanotechnology*; Bhushan, B., Ed.; Springer Netherlands: Dordrecht, 2012; pp. 90–93 ISBN 978-90-481-9751-4.
  31. MikroMasch Probes and Cantilevers Available online: [www.spmtips.com/library-probes-and-cantilevers.lib](http://www.spmtips.com/library-probes-and-cantilevers.lib) (accessed on 18 May 2021).
  32. Dewan, M.C.; Rattani, A.; Gupta, S.; Baticulon, R.E.; Hung, Y.-C.; Punchak, M.; Agrawal, A.; Adeleye, A.O.; Shrimel, M.G.; Rubiano, A.M.; et al. Estimating the Global Incidence of Traumatic Brain Injury. *Journal of Neurosurgery* **2018**, *130*, 1080–1097, doi:10.3171/2017.10.JNS17352.
  33. Park, K.; Biederer, T. Neuronal Adhesion and Synapse Organization in Recovery after Brain Injury. *Future Neurol* **2013**, *8*, 555–567, doi:10.2217/fnl.13.35.
  34. Paolicelli, R.C.; Bergamini, G.; Rajendran, L. Cell-to-Cell Communication by Extracellular Vesicles: Focus on Microglia. *Neuroscience* **2019**, *405*, 148–157, doi:10.1016/j.neuroscience.2018.04.003.
  35. Zhang, Y.; Chopp, M.; Zhang, Z.G.; Katakowski, M.; Xin, H.; Qu, C.; Ali, M.; Mahmood, A.; Xiong, Y. Systemic Administration of Cell-Free Exosomes Generated by Human Bone Marrow Derived Mesenchymal Stem Cells Cultured under 2D and 3D Conditions Improves Functional Recovery in Rats after Traumatic Brain Injury. *Neurochem Int* **2017**, *111*, 69–81, doi:10.1016/j.neuint.2016.08.003.



36. Dragovic, R.A.; Gardiner, C.; Brooks, A.S.; Tannetta, D.S.; Ferguson, D.J.P.; Hole, P.; Carr, B.; Redman, C.W.G.; Harris, A.L.; Dobson, P.J.; et al. Sizing and Phenotyping of Cellular Vesicles Using Nanoparticle Tracking Analysis. *Nanomedicine* **2011**, *7*, 780–788, doi:10.1016/j.nano.2011.04.003.
37. Théry, C.; Witwer, K.W.; Aikawa, E.; Alcaraz, M.J.; Anderson, J.D.; Andriantsitohaina, R.; Antoniou, A.; Arab, T.; Archer, F.; Atkin-Smith, G.K.; et al. Minimal Information for Studies of Extracellular Vesicles 2018 (MISEV2018): A Position Statement of the International Society for Extracellular Vesicles and Update of the MISEV2014 Guidelines. *J Extracell Vesicles* **2018**, *7*, doi:10.1080/20013078.2018.1535750.
38. Szatanek, R.; Baj-Krzyworzeka, M.; Zimoch, J.; Lekka, M.; Siedlar, M.; Baran, J. The Methods of Choice for Extracellular Vesicles (EVs) Characterization. *Int J Mol Sci* **2017**, *18*, doi:10.3390/ijms18061153.
39. Midekessa, G.; Godakumara, K.; Ord, J.; Viil, J.; Lättekivi, F.; Dissanayake, K.; Kopanchuk, S.; Rinken, A.; Andronowska, A.; Bhattacharjee, S.; et al. Zeta Potential of Extracellular Vesicles: Toward Understanding the Attributes That Determine Colloidal Stability. *ACS Omega* **2020**, *5*, 16701–16710, doi:10.1021/acsomega.0c01582.
40. Guthrie, J.W. 3.01 - General Considerations when Dealing with Biological Fluid Samples. In *Comprehensive Sampling and Sample Preparation*; Pawliszyn, J., Ed.; Academic Press: Oxford, 2012; pp. 1–19 ISBN 978-0-12-381374-9.
41. Parisse, P.; Rago, I.; Ulloa Severino, L.; Perissinotto, F.; Ambrosetti, E.; Paoletti, P.; Ricci, M.; Beltrami, A.P.; Cesselli, D.; Casalis, L. Atomic Force Microscopy Analysis of Extracellular Vesicles. *Eur Biophys J* **2017**, *46*, 813–820, doi:10.1007/s00249-017-1252-4.
42. TRPS Reagent Kit Available online: <https://store.izon.com/products/trps-reagent-kit> (accessed on 28 April 2021).
43. Nečas, D.; Klapetek, P. Gwyddion: An Open-Source Software for SPM Data Analysis. *Open Physics* **2012**, *10*, 181–188, doi:10.2478/s11534-011-0096-2.
44. Yuana, Y.; Oosterkamp, T.H.; Bahatyrova, S.; Ashcroft, B.; Garcia Rodriguez, P.; Bertina, R.M.; Osanto, S. Atomic Force Microscopy: A Novel Approach to the Detection of Nanosized Blood Microparticles. *J Thromb Haemost* **2010**, *8*, 315–323, doi:10.1111/j.1538-7836.2009.03654.x.
45. Skliar, M.; Chernyshev, V.S. Imaging of Extracellular Vesicles by Atomic Force Microscopy. *J Vis Exp* **2019**, doi:10.3791/59254.
46. Maas, S.L.N.; de Vrij, J.; van der Vlist, E.J.; Geragousian, B.; van Bloois, L.; Mastrobattista, E.; Schiffelers, R.M.; Wauben, M.H.M.; Broekman, M.L.D.; Nolte-’t Hoen, E.N.M. Possibilities and Limitations of Current Technologies for Quantification of Biological Extracellular Vesicles and Synthetic Mimics. *Journal of Controlled Release* **2015**, *200*, 87–96, doi:10.1016/j.jconrel.2014.12.041.
47. Osteikoetxea, X.; Sódar, B.; Németh, A.; Szabó-Taylor, K.; Pálóczi, K.; Vukman, K.V.; Tamási, V.; Balogh, A.; Kittel, Á.; Pállinger, É.; et al. Differential Detergent Sensitivity of Extracellular Vesicle Subpopulations. *Org Biomol Chem* **2015**, *13*, 9775–9782, doi:10.1039/c5ob01451d.
48. Anderson, W.; Lane, R.; Korbie, D.; Trau, M. Observations of Tunable Resistive Pulse Sensing for Exosome Analysis: Improving System Sensitivity and Stability. *Langmuir* **2015**, *31*, 6577–6587, doi:10.1021/acs.langmuir.5b01402.
49. Bachurski, D.; Schuldner, M.; Nguyen, P.-H.; Malz, A.; Reiners, K.S.; Grenzi, P.C.; Babatz, F.; Schauss, A.C.; Hansen, H.P.; Hallek, M.; et al. Extracellular Vesicle Measurements with Nanoparticle Tracking Analysis – An Accuracy and Repeatability Comparison between NanoSight NS300 and ZetaView. *Journal of Extracellular Vesicles* **2019**, *8*, 1596016, doi:10.1080/20013078.2019.1596016.
50. Akers, J.; Ramakrishnan, V.; Nolan, J.; Duggan, E.; Fu, C.-C.; Hochberg, F.; Chen, C.; Carter, B. Comparative Analysis of Technologies for Quantifying Extracellular Vesicles (EVs) in Clinical Cerebrospinal Fluids (CSF). *PLOS ONE* **2016**, *11*, e0149866, doi:10.1371/journal.pone.0149866.

## 8. Curriculum vitae

### PERSONAL INFORMATION

Ivona Vidović

📍 Selska 121F, Zagreb 10 000, Croatia

☎ +385 91 3441 795

✉ [ivona.vidovic@student.uniri.hr](mailto:ivona.vidovic@student.uniri.hr) / [ivvidovic97@gmail.com](mailto:ivvidovic97@gmail.com)

### WORK EXPERIENCE

4/2019-2020

*Supercomputer molecular dynamics training, student research assistant*

- ❖ Preparing molecular structures for the subsequent supercomputer analysis and visualisation afterwards. Trajectory analysis.

Željko M. Svedružić, PhD., assistant professor

Department of Biotechnology, University of Rijeka, Biomolecular Structure and Function Laboratory: <https://www.svedruziclab.com/>

2/12/2019-20/12/2019

*"Design of biologically active molecules by computer methods", student teaching assistant*

- ❖ Demonstrating the use of molecular analysis and molecular dynamics simulation software like UCSF Chimera, VMD, PyMOL, etc.

Željko M. Svedružić, PhD., assistant professor

Vedran Miletić, Ph.D. in computer science, senior lecturer at University of Rijeka Department of Informatics

Department of Biotechnology, University of Rijeka, Biomolecular Structure and Function Laboratory

### EDUCATION, TRAINING

2019-2021

*M.Sc. in Medicinal Chemistry (ongoing)*

Master's thesis

*"Nanotechnologies for size and concentration measurement of extracellular vesicles from human cerebrospinal fluid: comparison of atomic force microscopy and tunable resistive pulse sensing"*

- ❖ Specialised in visualisation and molecular processing softwares (Gwyddion, Nanoscope, VMD, UCSF Chimera)
- ❖ Acquired skills in Good laboratory practice (GLP), publication process and presentation of scientific results.

Mentor: Assoc. prof. MLadenka Malenica

Co-mentor: Dr. sc. Marko Perčić

Faculty of Medicine, University Departments - NANORI, Center for Micro- and Nano-Sciences, University of Rijeka

27/05/2019 - 07/06/2019

*Pharmaceutical company, student traineeship*

Department of Research and Development

Jadran Galenski Laboratory, Rijeka (Croatia)

2016-2019

*B.Sc. in Biotechnology and Drug Research* univ. bacc. biotech. et pharm. inv.

Department of Biotechnology, University of Rijeka

### PERSONAL SKILLS

Mother tongue(s)	Croatian				
Other language(s)	UNDERSTANDING		SPEAKING		WRITING
	Listening	Reading	Spoken interaction	Spoken production	
	English	C1	C2	C1	B2
	University coursework in English certified				
	Italian	C1	C1	B2	B2
	Istituto di lingua e cultura Italiana "Michelangelo", Firenze (C1)				
	German	A2	B1	A2	A2
	Levels: A1/2: Basic user - B1/2: Independent user - C1/2 Proficient user Common European Framework of Reference for Languages				
	Communication skills	❖ Actively participated in Youth in Policy Dialogue - Ljubljana (Slovenia) 4th National Selection Conference, as part of Erasmus + programme			
17/08/2018-22/08/2018	❖ Proficient communication skills gained through active discussions in <b>European Youth Parliament</b> sessions. ❖ Developed critical thinking skills, and improved <b>teamwork</b> capabilities.				
Organisational / managerial skills	<b>Vice-President</b> of the organizing committee				
6/2018	❖ 2 <sup>nd</sup> Student Congress of Environmental Health Faculty of Medicine, University of Rijeka				
25/08/21 – 29/08/21	Co-organized the <b>Chemistry summer school</b> for students				
	❖ Consisted of chemistry related lectures, organic chemistry practicum, visit to the Rijeka Oil Refinery - INA, dd ❖ Led by Assistant prof. Tomislav portada University Departments, University of Rijeka				
Computer skills	- Proficient user of Microsoft OS, Microsoft Office Suite - Independent user of <b>Linux OS</b> - Basic user of statistical analysis software: MedCalc, <b>R - R studio</b> - Independent user of software for molecular analysis and <b>molecular dynamics simulations</b> : UCSF Chimera, GROMACS, VMD, PyMOL, AutoDock Vina, GAMESS - Independent user of image processing software: Gwyddion, Nanoscope				
Contribution to society	Freelance poem and prose writer				
2/2020-today	❖ Colaboration with Croatian magazine for the homeless "Ulični Fenjer"				
21/01/20	Student Project "Naturis"				
	❖ Led a workshop on preparing natural deodorant Department of Biotechnology, University of Rijeka				

1/3/2017-15/4/2018

Extracurricular Italian teacher

- ❖ Taught Italian to elementary school children aged 7-11  
Rijeka City Library, Stribor Children's Department, Rijeka

Driving licence

B, AB

#### ADDITIONAL INFORMATION

##### Conferences and workshops

- ❖ *T. Portada* : Nuclear magnetic resonance spectroscopy, **NMR** workshop (03-05/05/21)
- ❖ [\*NEURI\*](#) : Student Congress of Neuroscience, **active** participation; poster on "*Nanotechnology-based quantifications of nanoparticles from human cerebrospinal fluid: comparison of Atomic Force Microscopy and Tunable Resistive Pulse Sensing*" (23-24/05/21)
- ❖ *Bruker* : Connect and Learn European **BioAFM** Users Meeting (13/01/21)
- ❖ *Jeol* : Out in the cold: **CryoTEM** (12/01/2021)
- ❖ *ERSTE & STEIERMÄRKISCHE BANK D.D Rijeka* : Department of Corporate social responsibility (June, July 2018)

##### Grants

- ❖ SIZIF Fund (Student Council of the University of Rijeka and the University of Rijeka Foundation)  
Funded student scientific research activities in Jožef Stefan Institute, Ljubljana (20/09/2021-02/10-2021)  
*Validation and optimisation of the 3 most commonly used methods for EV characterisation, using chromatographically isolated EVs: Nanoparticle Tracking Analysis (NTA), Dynamic Light Scattering (DLS) and Tunable Resistive Pulse Sensing (TRPS).*

##### Publications

Malenica M., Vukomanović M., Kurtjak M., Mascotti V., dal Zilio S., Greco S., Lazzarino, M., Krušić, V., Perčić, M., Jelovica Badovinac, I., Wechtersback, K., **Vidović**, I., Baričević, V., Valić, S., Lučin, P., Kojc, N., Grabšić, K.: *Perspectives of microscopic methods for morphology characterisation of extracellular vesicles from human biofluids*. Biomedical Materials and Nanomedicine. (2021) Biomedicines

**Vidović**, I., Kratožil, M., Debeljak, N., Luttenberger, L. R.: *Impact of COVID-19 on Croatian population during the first stage of infection and possibilities for building future resilience*  
~in process of review

**Vidović**, I., Luttenberger, L. R.: *The contribution of home composting to environmental protection*  
Polytechnica: Journal of Technology Education, Volume 3, Number 1 (2019) Scientific journal portal Hrčak